Research Square

Preprints are preliminary reports that have not undergone peer review.
They should not be considered conclusive, used to inform clinical practice,
or referenced by the media as validated information.

A phage encoded GapR nucleoid-associated protein binds a bacterial GapR to deactivate it via an inhibitory hetero-oligomer mechanism

Maria Schumacher

maria.schumacher@duke.edu

Duke University https://orcid.org/0000-0002-5264-1120

Raul Salinas

Duke University School of Medicine https://orcid.org/0000-0001-9011-683X

Sunny Yadav

duke university

Katie Leung

University of Washington

Porter Ellis

Duke University

Hengshan Zhang

duke university

Monica Guo

University of Washington https://orcid.org/0000-0002-6720-2323

Article

Keywords:

Posted Date: March 12th, 2026

DOI: https://doi.org/10.21203/rs.3.rs-8865587/v1

License: This work is licensed under a Creative Commons Attribution 4.0 International License.
Read Full License

Additional Declarations: There is **NO** Competing Interest.

A phage encoded GapR nucleoid-associated protein binds a bacterial GapR to deactivate it via an inhibitory hetero-oligomer mechanism

Maria A. Schumacher[1], Raul Salinas[1], Sunny Yadav[1], Katie Leung[2], Porter K. Ellis[1], Hengshan Zhang[1] and Monica S. Guo[2]

[1]Department of Biochemistry, 307 Research Dr., Box 3711, Duke University Medical Center, Durham, NC 27710, USA.

[2]Department of Microbiology, 750 Republican St., F830, University of Washington School of Medicine, Seattle, WA 98109, USA.

Correspondence:

E-mail: maria.schumacher@duke.edu

ABSTRACT

Nucleoid associated proteins (NAPs) play key roles in bacterial chromosome organization and cellular processes. Recent work identified GapR as an essential NAP that is ubiquitous in α-proteobacteria. GapR structures reveal that the dimeric form of GapR can tetramerize in the presence of DNA to form a DNA-encasing clamp and data showed that GapR is required for bacterial replication as it recruits topoisomerases to regions of overtwisted DNA. Interestingly, diverse phages that infect α-proteobacteria encode GapR homologs. To gain insight into how phage GapRs may impact their cellular homologs we performed structure/function analyses on the roseobacterial and roseophage RDJLΦ1 GapR proteins. Crystal structures revealed that the RDJLΦ1 GapR harbors a structure different from the bacterial GapR that is incompatible with DNA binding. Cellular localization and fluorescence binding assays confirmed that the RDJLΦ1 phage GapR does not bind DNA. Strikingly, data show that the RDJLΦ1 GapR and bacterial GapR can form hetero-oligomers, suggesting that the RDJLΦ1 GapR may function as a GapR poison. Indeed, assays showed that the heterodimer forms is unable to bind DNA. Collectively these studies indicate a mechanism by which a phage encoded NAP can derail a host NAP to co-opt the cell and possibly favor phage infectious processes.

INTRODUCTION

In all organisms, chromosomes must be compacted to fit within the confines of cells that are ~1000-fold smaller than the extended chromosomal DNA. In bacteria, chromosomal DNA is organized by a combination of factors that include DNA supercoiling, macromolecular crowding and a diverse group of DNA-binding proteins called nucleoid associated proteins (NAPs)[1-4]. NAPs are small, abundant and basic DNA binding proteins. Certain NAPs such as IHF and Fis can bind DNA with sequence specificity but most NAPs show either a preference for AT-rich DNA sites or interact with DNA in a non-sequence specific manner[5-9]. Hence, NAPs are structurally and functionally heterogenous. To organize the DNA, NAPs wrap, bend and/or bridge DNA. Notably, some NAPs are selectively encoded in certain bacteria. One such protein, GapR has been recognized as a "signature" protein, distinctive of the α-proteobacterial class[10] and data showed that it is essential in *Caulobacter*[10-16].

Like other NAPs, GapR is a small, basic protein, with the Caulobacter protein comprised of just 89 residues[10-16]. Studies demonstrated that it not only binds and organizes DNA, but recruits topoisomerase II proteins. In particular, GapR associates with positively supercoiled DNA, localizing topoisomerase II proteins to overtwisted regions of the chromosome where it is needed to relax positive supercoils[13]. This function is essential for productive DNA replication. Although GapR was found to have a preference for AT-rich DNA sequences[10-16], enrichment of GapR is also found at the 3′ end of highly expressed genes and operons[13] and hence GapR also impacts transcription. The ability

of GapR to recognize and bind over-twisted DNA has recently been leveraged as a tool to map positively supercoiled regions in bacterial and yeast genomes[17-19].

Insight into GapR function was provided by recent GapR crystal structures[13-15]. These studies showed that the apo GapR contains a unique fold consisting of two long helices[13-15]. In the structure, the N-terminal helix, α1, combines with α1 of a second GapR subunit to form an antiparallel coiled coil dimer. Strikingly, GapR-DNA structures revealed that GapR can further oligomerize to form a tetramer or dimer-of-dimers that creates a DNA binding clamp. In the structure, the DNA is completely encircled inside the central cavity of the clamp. This cavity is lined with basic residues that are conserved among bacterial GapR homologs[13-15]. To form the dimer-of-dimers, a break in the center of α2 of the apo structure is created, leading to the creation of two helices, α2 and α3, which are positioned at opposite ends of the α1-α1′ antiparallel coiled coil dimer. The α2-α3 helical pairs from each GapR subunit interdigitate with α2-α3 helical pairs from a second GapR dimer to form the dimer-of-dimers. These cross α2-α3 zipper interactions seal the ends of the dimer-of-dimers, creating the central DNA binding cavity. There are no base contacts observed in the structure, consistent with GapR binding DNA in a mostly non-sequence specific manner, with the AT-rich preference likely arising from the conformational flexibility exhibited by such DNA regions.

Although GapR proteins are ubiquitous in α-proteobacteria, they are not found in other bacterial or eukaryotic lineages[10,20]. Interestingly, however, many GapR homologs are encoded in bacteriophages that infect α-proteobacteria[10]. To replicate, phages hijack the

cellular machinery of their bacterial hosts to favor the production of progeny phage. The presence of GapR genes in many α-proteobacterial phages suggests the possibility that they may have been acquired by phages for purposes favoring their propagation. In fact, multiple bacteriophages and mobile genetic elements (MGEs) have now been shown to encode homologs of the diverse NAPs of the bacteria they infect, indicating that this is a widespread phenomenon[21-29]. What function(s) most of these phage NAPs play, however, is not well understood at the molecular level.

To gain insight into phage GapR structure and function we aligned the sequences of bacterial and phage encoded GapR homologs. These analyses showed that most phage GapRs showed strong sequence homology to bacterial GapR proteins, with the exception of GapR proteins encoded by some of the lytic roseobacterial phages of the *Siphoviridae* class that use *Roseobacter denitrificans* as a host. The *Roseobacter* clade is a large group of bacteria, consisting of more than 70 genera and 170 species[30-32]. These bacteria are mainly marine organisms, accounting for ~25% of coastal marine bacteria. This group of bacteria is important from ecological and biomedical standpoints as members have been shown to degrade pollutants and produce a wide range of bioactive secondary metabolites[30-32]. The roseophages that infect these bacteria play critical roles in regulating community structure, metabolic activities and the evolution of roseobacters[33-34]. Consequently, understanding these bacteria, their life cycles and phages that infect them is of interest. Thus, we undertook structural studies on the roseobacterial GapR and the GapR from the well characterized roseophage, RDJLΦ1[33-34]. Structures of the RDJLΦ1 GapR revealed it forms a dimer that, while containing a central α1 coiled coil similar to

bacterial GapRs, differs from the bacterial GapR structures in a way that would be incompatible for the mode of DNA binding observed in bacterial GapRs. Indeed, our data demonstrate that the RDJLΦ1 GapR cannot bind DNA. Strikingly, we also showed that the RDJLΦ1 GapR interacts with the roseobacterial GapR and that the resultant heterocomplex does not bind DNA. Thus, RDJLΦ1 GapR acts as a poison for the DNA binding function of the bacterial GapR protein.

RESULTS

Crystal structures of the RDJLΦ1 GapR protein

Bioinformatic analyses of GapR proteins revealed that homologs are encoded in the genomes of several phage that infect α-proteobacterial species. Interestingly, the alignments show that most of the phage GapR homologs show a high degree of sequence homology to the bacterial GapRs and in particular, contain residues previously shown to be important in DNA binding, including Lys42, Lys50, Lys56, Lys63 and Lys66 (using *C. crescentus* numbering) (Fig. 1). By contrast, putative GapR homologs encoded by roseophages in the *Siphoviridae* class of phages (RDJLΦ1, RDJLΦ2, RDJL6, and RDCBΦ1) are sequentially very similar to each other but show significant sequential differences to the bacterial GapR proteins. Moreover, they lack key DNA binding basic residues in positions 42,49, 56 and 66 (Fig. 1). Hence, we sought to investigate the GapR encoded by the well characterized roseophage, RDJLΦ1[33-34].

Given the sequential differences between this phage GapR and the bacterial GapR proteins (sharing less than 25% sequence identity), we first sought to first obtain a

structure of the 83 residue RDJLΦ1 GapR protein. We obtained crystals of the RDJLΦ1 GapR protein and collected X-ray intensity data to 2.2 Å resolution. Attempts to solve the structure using previously solved GapR coordinates in molecular replacement (MR) failed (35). This suggested the possibility that the RDJLΦ1 GapR protein may adopt a different overall structure from the bacterial GapR proteins. Thus, to obtain unbiased *de novo* phases we carried out single wavelength anomalous diffraction (SAD) experiments on crystals grown with selenomethionine substituted RDJLΦ1 GapR protein. These data produced an excellent SAD map (Fig. 2A) that allowed model building and the constructed structure was refined to final R_{work}/R_{free} values of 23.1%/25.6% to 2.20 Å resolution (Fig. 2B-D; Table S1).

The RDJLΦ1 GapR structure contains a central dimerization, coiled coil generated by contacts between two-fold related helices, α1 and helix α1' (where ' indicates other subunit in the dimer), that is similar to the α1/α1' interaction observed in the bacterial GapR structures (Fig. 3). However, unlike the apo bacterial GapR structure in which α1 is followed by an elongated α2 helix, in the RDJLΦ1 GapR structure two helices, α2 and α3, follow α1, with helices 2 and 3 forming contacts with α1' (Fig. 3). In the latter interaction three leucines, Leu10, Leu14 and Leu17 from α1 insert into a hydrophobic pocket formed by the packing of α2' and α3' (Fig. 2D). For the α1/α1' dimer interaction, two isoleucine residues, Ile24 and Ile27, appear crucial as they are located at the center of the coiled coil and their hydrophobic interactions fasten the two α1 helices together. Two-fold related hydrogen bonds formed between Glu21 and Lys31 further stabilize the coiled coil dimer (Fig. 2C). The residues that mediate these dimer contacts in the RDJLΦ1

GapR dimer are notably conserved among the *Siphoviridae* roseophage GapR homologs with the exception that in the RDCBΦ1 phage GapR, Ile24 and Ile27 are replaced with valine and leucine residues, respectively, which could play the same role as the Ile residues (Fig. 1). The RDJLΦ1 GapR structures also differs from the DNA-bound structure of GapR as although DNA binding to the bacterial GapR induces a break in α2, the resultant α3 is positioned differently in the bacterial GapR structure compared to the RDJLΦ1 GapR structure (Fig. 3).

Because the RDJLΦ1 GapR structure was different from those of the bacterial GapRs, to assess if it might be a crystallization artifact we next obtained a second RDJLΦ1 GapR crystal form under different crystallization conditions that exhibited different packing. This structure, which was solved to 3.0 Å resolution, revealed the same dimer as observed in our other RDJLΦ1 GapR structure, whereby each subunit contains 3 helices. Indeed, the structures overlay with a root mean squared deviation (RMSD) of 0.6 Å (Fig. 4A).

Comparison of RDJLΦ1 GapR and bacterial GapR structures

Structural homology searches using SSM/PDBfold revealed that there are no structures in the protein data bank with a fold similar to the RDJLΦ1 GapR structure; unsurprisingly, the structures with the strongest homology are the DNA-bound forms of bacterial GapR structures. However, the structural homology between the RDJLΦ1 GapR and GapR-DNA structures is weak, with RMSDs of 5.1 Å, 4.0 Å and 5.3 Å for superpositions of 61, 52 and 61 Cα atoms, respectively (pdb codes: 6OZZ, 6CG8 and 6OZY).

The primary structural similarity between the RDJLΦ1 and bacterial GapR structures inlcudes helix α1 and the first few turns of α2 (Fig. 4B-E; Fig. 5). The RDJLΦ1 GapR structure contains an α1 of similar length to the bacterial GapR α1 and a turn leading to α2. The turn between α1 and α2, is formed by Gly42 in the RDJLΦ1 GapR. This glycine is notably also conserved in the bacterial GapR structures (Fig. 4B-E). In fact, this glycine is one of the only residues that is completely conserved among all bacterial and phage GapRs, consistent with the presence of a loop between α1 and the N-terminal region of α2 in these structures (Fig. 4B-E). Thus, this α1-loop-α2 region can be defined as a signature feature of all GapR homologs (Fig. 4B-E). However, the structure following α1 and the first three turns of α2, differs significantly between the structures of RDJLΦ1 GapR and both states of the bacterial GapRs (Fig. 3) and consistent with this finding, the sequences in these regions are also the most divergent among GapR homologs (Fig. 1).

Strikingly, when we overlaid the RDJLΦ1 GapR structure onto the DNA bound form of the bacterial GapR we found that the α3 helix in the RDJLΦ1 GapR structure superimposes onto the α3 helix in the bacterial GapR that is formed upon DNA binding. In the bacterial GapR this α3 helix, in fact, comes from the other dimer in the dimer-of-dimers (Fig. 3; Fig. 4F). Thus, the RDJLΦ1 GapR dimer appears autoinhibited for DNA binding. The differences in the phage and bacterial GapRs structures in this region appears to arise from sequential differences between the proteins (Fig. 1). In particular, in the bacterial GapRs the long α2 found in the apo state is broken during DNA binding as facilitated by the central Asp68 residue (in the *Caulobacter* structure), which functions as a helix N-cap, stabilizing the newly formed α3 (Fig.4B-E). The residue corresponding to this

aspartic acid is highly conserved in most bacterial GapR sequences but when it is not, it is replaced by asparagine or serine, which along with aspartic acid, are the most efficient residues for mediating N-capping, with glutamic acid, also observed in some GapRs, also capable of N-capping. In the RDJLΦ1 GapR and other roseophage GapRs, the aspartic acid is replaced by a glycine, Gly58 (Fig. 1; Fig. 4B-E), which forms a stable loop that does not require it be induced by DNA binding. This turn/loop region in the RDJLΦ1 GapR structure is also longer than the short helical break between α1 and α2 observed in the bacterial GapRs (compare Fig. 4B and C).

Test of the RDJLΦ1 GapR structural model

Though the same RDJLΦ1 GapR structure was observed in two distinct crystal forms, to test the structural model we next performed biochemical assays. The structures indicate that RDLJΦ1 GapR is dimeric. Hence, we performed size exclusion chromatography (SEC) to analyze the oligomeric state of the protein in solution. These experiments showed that the wild type (WT) RDJLΦ1 GapR (at 70 μM) eluted at a predicted molecular weight (MW) of 28 kDa, which is consistent with a dimeric structure (calculated MW for the His-tagged protein was 25 KDa) (Fig. 6A). To test the model in more detail we generated a RDJLΦ1 GapR(I24E-I27E) mutant as the structure indicates these residues are key in dimer formation. SEC experiments revealed that the mutant protein eluted solely as a monomer (Fig. S1A). We also utilized glutaraldehyde crosslinking to assess dimer formation. In these experiments, while the WT phage GapR formed dimers, the mutant protein showed no crosslinking, again supporting it does not form dimers (Fig. S1B).

We considered that the phage GapR may be present at low to high nM concentrations in cells (lower than the 70 μM used in SEC). Thus, to probe the RDJLΦ1 GapR oligomeric state at lower concentrations we employed mass photometry (MP), which allows MW analyses at nM concentrations[37-38]. Because MP experiments provide determinations of MWs of molecules in the range of 30 kDa to 5 MDa, the WT GapR is too small to be analyzed by this method. Hence, we expressed the RDJLΦ1 GapR as a fusion protein with an N-terminal Maltose binding protein (MBP) tag (Methods). Similar fusion protein strategies have been used to assess oligomerization of small proteins by MP[39]. For these experiments, we engineered a long linker between MBP and the RDJLΦ1 phage GapR protein to prevent possible interactions between the two. MBP was also utilized for this purpose because it is monomeric and adds 42.5 kDa in molecular weight (MW) [40]. Thus, the MBP-RDJLΦ1 GapR monomer has an expected MW of ~48 kDa.

MP analyses were peformed first by taking a stock of MBP-RDJLΦ1 at 100 μM and then diluting immediately before MP analyses. The analyses of the data revealed that most of the sample, 72%, was present as a dimer species. However, monomers were also present and accounted for 23% of the sample (Fig. 5B). To assess whether the oligomeric state of the phage GapR shows an increase in MW consistent with DNA binding, we included 20mer DNA (top strand: 5´-ATTATTAATTAATTAATAAT-3´) in the MBP-RDJLΦ1 GapR sample at a concentration of 150 nM; previous studies had shown that bacterial GapR proteins can bind DNA sites that contain a minimum of 10 bp[13]. The resultant data, however, was similar to the non-DNA added results with most of the protein

present as a dimer (71%) and 19% as monomers (Fig. 5B), suggesting that DNA does not bind RDJLΦ1 GapR, at least under these conditions.

Interestingly, when we allowed the diluted MBP-RDJLΦ1 GapR protein to equilibrate for several hours at 25 nM and then performed MP we found that that most of the sample, 69%, was present as monomers (47 ± 8.1 kDa) with 26% present as dimers (97 +/- 9.2 kDa) while ~5% was present as a mixture of higher order particles, likely aggregates (Fig. 5C). These data indicate that RDJLΦ1 GapR is in an equilibrium between monomer and dimer forms.

Structure of the Roseobacterial GapR protein

The finding that the RDJLΦ1 GapR has a different structure from the apo *C. crescentus* GapR led us to question if the chromosomal Roseobacterial GapRs might also have a different structures than the previously solved bacterial GapR structures from *Caulobacter* and *Bosea* sp. Root381[13-15]. Hence, we obtained crystals of the apo Roseobacterial MED193 sp. GapR (which is 90% identical to *R. denitrificans* GapR) and solved the structure (Table S1). The structure revealed the same dimeric conformation and overall subunit fold observed for the apo *C. crescentus* GapR whereby each subunt is comprised of two helices (Fig. 6A).

We also solved a structure of the *R. denitrificans* GapR bound to a 18mer DNA site (5'-ATAATTAATTAATTAATTAT-3'). The structure was determined to 2.9 Å resolution and revealed the same dimer-of-dimers clamp structure observed in the *C. crescentus* GapR-

DNA structure (6CG8) (Fig. 6B-C)[13]. While the *R. denitrificans* GapR-DNA crystals could not be grown in the absence of DNA, density for the DNA was not evident. As the GapR-DNA structure was solved by MR, we sought to obtain *de novo* phases to see if the resultant electron density maps would reveal DNA density. Because the *R. denitrificans* GapR contains a cysteine we performed heavy atom soaks with mercuric chloride. Highly redundant data were collected and a SAD anomalous peak calculated from the data confirmed that the cysteine had been modified (Fig. S2A-D). *De novo* phased electron density maps, while revealing clear density for the GapR protein (Fig. S2B) did not show density for DNA. Hence, the data indicate that the DNA is likely disordered in the structure, which is often the case for non-sequence specific DNA binding proteins.

DNA binding analyses of *R. denitrificans* and RDJLΦ1 phage GapR

A striking finding from the structure of the RDJLΦ1 GapR is that it appears to be in a conformation that is incompatible with DNA binding (Fig. 4F). However, to directly test whether the RDJLΦ1 GapR protein can bind DNA we employed fluorescence polarization (FP) and analyzed binding to an double stranded AT-rich DNA oligonucleotide (top strand: 5´-ATTATTAATTAATTAATAAT-3´). In these assays, the RDLJΦ1 GapR showed no binding to the AT-rich DNA site, even at high concentrations, while the *R. dentrificans* GapR bound saturably to the DNA oligo with a K_d of 150 +/- 23 nM (Fig. 6D). We next investigated if the phage GapR might bind to a dsDNA, fluoresceintly tagged GC-rich DNA site (top strand: 5´-CGCGCCGGCCGGCCGGCGCG-3´). Like the AT-rich 20mer site, the RDJLΦ1 GapR showed no binding to this DNA site (Fig.S3). The *Roseobacter* GapR bound this DNA, but with significantly reduced affinity (K_d=1 +/- 0.1 μM), compared

to the AT-rich 20mer. These data are consistent with previous studies showing bacterial GapRs bind DNA with a preference for AT-rich DNA[10-16].

Our data showed that the roseobacterial GapR binds DNA similar to the *C. crescentus* GapR[13]. However, our structure of Roseobacterial GapR bound to DNA did not reveal density for DNA. To assess if the Roseobacterial GapR makes the same contacts to the DNA as observed in the *C. crescentus* protein and hence employs the same DNA binding mechanism, we mutated *R. denitificans* GapR residues, Lys46, Arg54 and Lys68, that correspond to DNA-binding *Caulobacter* residues, Lys42, Lys50 and Lys74[13]. We substituted these residues to aspartic acids in the *R. denitrificans* GapR and performed FP assays with the 20-mer AT-rich DNA site. In these assays, the GapR(K46D-R54D-K68D) triple mutant protein showed no binding to DNA (Fig. 6D), supporting that the *R. denitrificans* GapR likely employs the same mechanism of DNA binding as the *C. crescentus* GapR protein.

Chromosomal DNA binding by roseobacterial and roseophage GapRs

Our MP and FP analyses showd no evidence of DNA binding by RDJLΦ1 GapR. However, these assays were done with short DNA sites that also lacked supercoiling, which might be necessary for binding by RDJLΦ1 GapR. Experiments where GapR protein was expressed in *E. coli* cells were previously used to analyse chromosomal DNA binding and cellular localization of GapR *in vivo*[11]. *E. coli* not only lacks a GapR homolog, but is an excellent model system to study nucleoid binding as unlike *C. crescentus,* DNA fluorophores used to label the nucleoid do not produce signal in the *E. coli* cytoplasm.

Thus, to analyze nucleoid DNA binding by the roseobacterial and RDJLΦ1 phage GapRs, we carried out confocal microscopy studies of tagged proteins expressed in *E. coli* (Methods).

For these studies we utilized eGFP-tagged Roseobacterial GapR and mCherry-tagged phage GapR. The eGFP-tagged Roseobacterial GapR expressed in *E. coli* was shown to colocalize with the DAPI stained nucleoid (Fig. 7A). The mCherry-tagged RDJLΦ1 GapR signal, by contrast, was confined to the cytoplasm (Fig. 7B). These data are consistent with our FP data indicating that the RDJLΦ1 GapR does not bind DNA. Interestingly, the cells expressing the RDJLΦ1 GapR appeared to be elongated or filamentous compared to WT. This suggests that overexpression of the phage protein may somehow impact *E. coli* cell division. Nonetheless, these studies and the FP data collectively indicate that while the Roseobacterial GapR binds DNA similar to *Caulobacter* GapR, the RDJLΦ1 phage GapR does not. Interestingly, co-expression of the mCherry-RDJLΦ1 GapR and the eGFP Roseobacterial GapR in *E. coli* revealed signal overlap, (Fig. 7C) which suggests possible interaction between the two proteins. However, because the proteins were significantly overexpressed it was difficult to discern specific colocalization and hence binding or interaction between the two GapR proteins.

RDJLΦ1 GapR and roseobacterial GapR hetero-oligomerize

Our confocal data suggested the possibility that the Roseobacterial and phage GapR proteins might interact. In this regard it is nteresting that our MP data revealed that there is a large percentage of monomer present in RDJLΦ1 GapR samples at mid to high nM,

which is close to physiological concentrations. This supports the possibility that the RDJLΦ1 GapR would be capable of exchange to form interactions with the roseobacterial protein. Using our crystal structures of both proteins, we performed modeling studies to ascertain if a heterodimer could be stably formed between the proteins. These modeling exercises indicated that one subunit of the roseobacterial GapR can indeed, heterodimerize with the phage GapR without clash (Fig. 8A). However, for hetero-oligomer formation, the roseobacterial GapR must also be present in an equilibrium between monomer and higher order oligomeric states to allow for the possible exchange. To investigate this we peformed MP analyses on the MBP-tagged Roseobacterial *R. denitrificans* GapR. The results showed that after transferring the sample from 4 ºC to room temperature (rt) for 1 h and then performing MP analyses, at concentrations of 200 nM, 48% of the MBP-*R. dentrificans* GapR was present as monomers with 20% dimer and 22% dimer-of-dimers (Fig. 8B). At 100 nM, there was 69% monomer, 9% dimer and 16% dimer-of-dimers. At a concentration of 50 nM, most of the protein was monomeric (71%), with 6% dimer and 19% dimer-of-dimers and finally at the lower concentration of 25 nM, 83% of the protein was monomeric with just 12% dimer-of-dimer (Fig. 8B).

Thus, the MP analyses show that at mid to low nM, most of the *R. dentificans* protein is monomeric in solution. The data also showed that the protein can form dimer-of-dimers even without added DNA, which is consistent with previous data[14]. But the dimer-of-dimers species might also have arisen from the presence of low amounts of contaminating DNA (despite our efforts to remove such contaminants), as previous studies have reported removal of contaminating DNA from GapR preparations is

challenging[11,13]. Nonetheless, the samples show that the protein at these concentrations is in an equilibrium between monomeric and oligomeric states. When we incubated the protein at rt for 4 hr (Fig. S4) we noted that there was a shift to more monomer; at 200 nM, there was 66% monomer, 10% dimer and 19% dimer-of-dimer. At 100 nM there was 71% monomer, 5% dimer and 19% dimer-of-dimer. At the lower concentrations of 50 nM, there was 70% monomer and 19% dimer-of-dimer while at 25 nM there was now 86% monomer with no detectable dimer or dimer-of-dimer (Fig. S4). In *Caulobacter*, it has been estimated that there are around 3000 molecules per cell, which for dimer and dimer-of-dimers, would place the intracellular concentration in the high nM concentrations. The *in vivo* temperature in cells is higher than rt, which would also lead to more monomers as our data shows increased temperature shifts equilibrium to the monomer state. Thus, this information combined with our MP data, showing significant monomer percentages of both the phage and roseobacterial GapRs, provide a mechanistic basis for hetero-oligomer formation.

To test for interactions between the RDJLΦ1 GapR and *Roseobacter* GapR proteins we next performed a bacterial two-hybrid analysis (B2H) based on the reconstitution of the split *Bordetella pertussis* adenylate cyclase[41]. Briefly, “bait” and “prey” proteins were fused to either the T18 or T25 fragment of adenylate cyclase and co-expressed in *E. coli* (Fig. 8C; Fig. S5A; Table S2). Protein-protein interactions between bait and prey reconstitutes adenylate cyclase, driving the synthesis of cyclic-AMP and leads to a red colony coloring on MacConkey agar plates. As a control we first used this assay to test self-oligomerization by *R. denitrificans* GapR and RDJLΦ1 GapR proteins as C-terminal

fusions (Fig. 8D). Both these proteins self-oligomerized and did not hetero-oligomerize with the fragments of adenylate cyclase (Fig. 8D, Fig. S5B). Next we asked whether *Roseobacter* and RDJLΦ1 GapR interact. We find that *Roseobacter* GapR can indeed interact with RDJLΦ1 GapR (Fig. 8D). We further confirmed this interaction by repeating all experiments as N-terminal fusions to adenylate cyclase subunits, finding that *Roseobacter* and RDJLΦ1 GapR form homo- and hetero-oligomers in all orientations (Fig. S5B).

Given the sequence similarity between Roseobacterial GapR and other bacterial and phage GapR, we wondered if RDJLΦ1 GapR could form hetero-oligomers with GapR from more diverse bacteria and phage. To test this idea, we asked if *Roseobacter* and RDJLΦ1 GapR are capable of binding to GapR from *Caulobacter* and its phage Cr30, JessA, and RW. To our surprise, we find that C-terminally tagged *Roseobacter* and RDJLΦ1 GapR form hetero-oligomers with *C. crescentus* GapR and Cr30 and JessA GapR (Fig. 8E). Neither *Roseobacter* and RDJLΦ1 GapR interacted with RW GapR, suggesting that RW GapR may act differently from these other homologs. Together, our data suggests that highly diverse bacterial and phage GapR interact.

RDJLΦ1-Roseobacter GapR heterodimers do not bind DNA

Our data showed that the RDJLΦ1 and *Roseobacter* GapR proteins interact. Interestingly, the hererodimer modeling in Fig. 8A suggests that the presence of one RDJLΦ1 GapR subunit in the heterodimer would prevent DNA binding due to the presence of the RDJLΦ1 α3 helix. This helix overlaps where the α3 helix from the dimer-of-dimer would bind, thus

inhibiting the formation of the DNA-binding dimer-of-dimers. To test this hypothesis we performed FP studies. First we prepared a mixture of RDJLΦ1 GapR and *R. denitrificans* GapR at low concentration and ran FP assays. The results showed that this complex, indeed showed essentially no binding to the AT-rich 20mer (Fig. 8F). To ensure, however, that the heterodimer contained stoichiometric amounts of RDJLΦ1 GapR and *R. denitrificans* GapR (i.e. a 1:1 complex) we constructed a RDJLΦ1 GapR-*R. denitrificans* GapR chimera. Our modeling showed that the C-terminus of the RDJLΦ1 GapR in the heterodimer would be proximal to the N-terminus of the Roseobacterial GapR (Fig.8A). Hence, we generated a RDJLΦ1 GapR-(GGSLVPRSHGGS)-Roseobacterial GapR chimera, which contains an linker with a thrombin cleavage site between the RDJLΦ1 and *Roseobacter* GapR proteins. The protein was expressed, purified and thrombin cleavage produced a stoichometric dimer. FP binding assays with this complex also showed essentially no binding to the 20mer DNA site (Fig. 8F). These data show that interaction with the RDJLΦ1 GapR protein prevents DNA binding by the *Roseobacter* GapR protein.

DISCUSSION

NAPs make key contributions to bacterial chromosome organization. But it has become increasingly appreciated that these proteins also play central, sometimes essential, roles in multiple DNA processes such as replication and transcription[21-29]. GapR is a NAP that was shown to be required for proper DNA replication in *C. crescentus* via its ability to recruit type II topoisomerases to replication forks[13]. Because GapR is essential, it was of interest that multiple α-proteobacterial phages were found to encode GapR homologs and it was suggested that the phage GapR proteins might somehow impact GapR

function[10]. However, the structure and function of phage GapRs have not been investigated in detail. Notably, recent work has highlighted that, in fact, many NAP and NAP-related proteins are encoded in mobile genetic elements (MGE), including bacteriophages[42], thus sparking interest in understanding their possible roles in phage and bacterial biology.

The molecular details behind phage encoded NAP proteins are currently not well understood. Indeed, there are only a handful of high-resolution structures reported of phage encoded NAPs. Interestingly, many of these include proteins that do not have homologs in their bacterial hosts and thus have been labeled as nucleoid-associated proteins (NAPs) based on their DNA-organizing roles. Examples of these phage NAP-like proteins include the λ phage RexA protein and Mu phage Mor protein[44-45]. The structure of RexA revealed it harbors a fold with a two-domain architecture that has homology to recombination proteins[44]. This structure suggests roles in non-specific DNA binding and also as a possible sensory protein. The Mu Mor protein exists as a dimer with a C-terminal helix-turn-helix DNA-binding domain. However, recent data suggests that Mu functions primarily as a transcription factor and hence may not act as a NAP[45]. A phage-encoded NAP that has been structurally characterized and shows homology to a bacterial NAP is the Pyophage Fis-like protein, NinH, the structure of which revealed a homodimer that binds DNA via the major groove in a manner similar to Fis[28].

While structural analyses are in their early stages, several studies have started to shed light on phage and MGE encoded NAP functions. Phage-encoded NAPs that have been

particularly well studied include the MotB protein from the T4 phage infecting *E. coli*[22] and H-NS-like phage proteins. For MotB, work in the Hinton lab has demonstrated that this protein functions to compact the host nucleoid, thus creating more room for T4 phage processes such as replication and packaging as well as causing global changes in gene expression[22]. A main line of defense by bacteria against MGEs, such as phages, is the silencing of foreign DNA. The H-NS protein and H-NS homolog Lsr2 play central roles in this process, so it is perhaps not surprising that many phage NAPs have evolved to target host H-NS proteins. In particular, studies have shown that truncated H-NS (H-NST) phage derivatives, which lack the H-NS C-terminal DNA binding domain, act as antagonists of H-NS function by impeding its correct oligomerization[21,23-26;45-49]. For example, the phage LUZ24 protein gp4 modulates the *P. aeruginosa* H-NS family member MvaT by targeting the formation of bridged DNA complexes[23]. While data has not been obtained to show a direct interaction, MotB was also shown to impair H-NS function[22]. Other MGE proteins homologous to the bacterial H-NS include the H-NSB and Hfp proteins from the serU-island of uropathogenic *E. coli* strains[45-46] and the Ler protein from the Locus of Enterocyte Effacement[47] pathogenicity island of enteropathogenic *E. coli* (EPEC). By acting as interaction partners for H-NS, MGE-encoded proteins directly impact the repressive function of the host-encoded H-NS proteins with either anti-silencing or co-repressor effects[45-49].

Like H-NS, GapR is an essential protein and hence interactions that either inhibit or alter its activity can have profound effects on host biology. Our studies on the RDJLΦ1 GapR reveal that, similar to several MGE encoded H-NS and H-NS-like proteins, this protein

affects the function of the bacterial encoded GapR by forming hetero-oligomers with it to impact its activity. Moreover, we obtained structural data that revealed the molecular mechanism (Fig. 9). Specifically, our data revealed the RDJLΦ1 GapR forms a different structure from the bacterial GapR proteins whereby it exsits in a inhibited form for DNA binding. Remarkably, however, the two proteins share similar α1–α1' coiled coil dimerization modules that provides the foundation for the formation of heteroligomers. But the resultant positioning of the α3 helix from the RDJLΦ1 GapR in the hetero-oligomer, prevents formation of a DNA binding active clamp. Interestingly, our bioinformatic analyses along with molecular modeling indicate that the GapR proteins from the roseobacterial infecting phages RDJLΦ2, RDJL6, and RDCBΦ1 appear to have the same structure as the RDJLΦ1 GapR and hence likely function similarly. To date only a handful of roseophages have been isolated and characterized, hence it is possible that there are GapR proteins similar to that encoded by RDJLΦ1 waiting to be discovered.

The RDJLΦ1, RDJLΦ2, RDJL6, and RDCBΦ1 phages form a specific phylogenetic clade that is distinct from other roseophages, such as the N4-like or DSS3Φ8 phages[33-34]. These phages all infect *R. denitrificans*, illustrating a shared host range that is different from roseophages targeting different host species or strains. Perhaps then not unexpectedly, these phages share significant nucleotide sequence identity and a high proportion of homologous genes, indicating a recent common ancestor. This contrasts with the highly mosaic nature and diversity seen when comparing across different roseophage lineages, which tend to only share a limited, core set of genes. Of particular note, the RDJLΦ1, RDJLΦ2, RDJL6, and RDCBΦ1 phages also appear to follow a

specific replication strategy that differs from other phages, which may reflect different requirements for topoisomerases or DNA structure, both of which are controlled by GapR proteins. This suggests an attractive mechanism by which these roseophage GapR proteins may help subvert the cell for phage production whereby the phage GapR binds and inhibits the DNA binding activity of the host GapR, including preventing it from targeting topoisomerases to replication forks. This would halt host DNA replication allowing the phage replication system to prevail in phage particle generation.

How other phage encoded GapRs may function is currently unclear. Indeed, to date, only 33% of the known Roseophages belong to *Siphoviridae* family (now classified in the class *Caudoviricetes*) and the rest to the families *Podoviridae* and *Microviridae*[50-51]. These latter roseophage GapRs and most sequenced phage encoded GapRs, show strong sequence homology to the bacterial counterparts, including the basic residues shown to be important in DNA binding. Future studies will be needed to assess possible roles of these phage encoded GapR proteins.

In conclusion, our studies on the Roseobacteriophage RDJLΦ-1 GapR have uncovered a unique structure for this NAP distinct from the bacterial homolog. This roseophage GapR structure notably adopts a state that is autoinhibited for DNA binding. Our biochemical studies support this finding. Thus, collectively, these analyses show that the RDJLΦ1 phage GapR utilizes a novel heterodimer inhibitory mechanism to associate with the bacterial GapR and prevent its DNA binding activity.

METHODS

Bacterial growth conditions

Escherichia coli strains were grown in LB (5 g/L NaCl, 10 g/L tryptone, 5 g/L yeast extract) at 37 °C with shaking at 200 rpm. Antibiotics were supplemented as needed (carbenicillin: 50 µg/mL liquid and 100 µg/mL plate and kanamycin: 30 µg/mL in liquid and 50 µg/mL in plates). The optical density was measured at 600 nm using an Eppendorf BioPhotometer. For bacterial two-hybrid assays, *E. coli* BTH101 was grown in M63 minimal media (0.4 g/L ammonium sulfate, 2.72 g/L monopotassium phosphate, 0.1 mg/L ferrous sulfate heptahydrate pH 7.0, 1 mM magnesium sulfate, 0.2% (w/v) maltose, 0.4% (w/v) glucose, and 0.0001% (w/v) vitamin B1) supplemented with carbenicillin, kanamycin, and 1 mM IPTG for 48 hours (h) at 30 °C with shaking before spotting on MacConkey agar (BD Difco) plates.

Expression and purification of RDJLΦ1 phage GapR and *Roseobacterial* GapR

The genes encoding full length (FL) RDJLΦ1 phage GapR, *Roseobacter denitrificans* GapR(12-100), MBP-FL RDJLΦ1 GapR (MBP residues 1-374-PPGSSGGLVPRGSHGGSS-FL RDJLΦ1 GapR), MBP- *Roseobacter denitrificans* GapR (MBP residues 1-374-PPGSSGGLVPRGSHGGSS-*R. denitrificans* GapR), *Roseobacter* MED193 sp. GapR (residues 9-87), *R. denitrificans* GapR(K46D-R54D-K68D), FL RDJLΦ1 GapR(I24E-I27E) and FL RDJLΦ1 GapR-GGSLVPRGSHGGS- *R. denitrificans* GapR chimera were purchased from Genscript Corporation as codon optimized genes for *E. coli* expression and subcloned into pET15b (all *R. dentrificans* constructs included residues 12-100 as the first 11 residues are predicted to be disordered). The resultant

expressed proteins have thrombin cleavable N-terminal His-tags for purification (Piscataway, NJ, USA;http://www.genscript.com). *E. coli* C41(DE3) cells were transformed with the expression vectors. For protein expression, cells were grown at 37 °C in Luria-Bertani (LB) medium with 0.10 mg/mL ampicillin to an OD_{600} of 0.3-0.4, then induced with 1 mM isopropyl β-d-thiogalactopyranoside (IPTG) at 15 °C overnight.

The purification strategy used was the same for all proteins. Cells with expressed proteins were harvested by centrifugation (each purification was 9 liters) and then resuspended in 100 mL of Buffer A (50 mM Tris-HCl pH 7.5, 800 mM NaCl, 5% (v/v) glycerol, 5 mM $MgCl_2$, 0.5 mM β-mercaptoethanol (βME)). Each 100 mL of resuspended cells were incubated for 30 min at 4°C (while stirring) with 200 µL protease inhibitor cocktail stock (100 µM aprotinin, 1 mM leupeptin, 1 mM pepstatin A) (Roche) and 40 U of a solution of 100 mg/mL DNase I (Roche). The resuspended cells were disrupted, first by sonication and then by microfluidizer. Cell debris was removed by centrifugation at 18,600 g at 4 °C for 60 min. Supernatants were loaded onto a cobalt NTA column (TALON Superflow histidine-tagged protein purification resin). The cobalt NTA columns were generated by pouring the resin into a Bio-Rad glass column and equilibrating before addition of the protein containing lysate and an overnight wash with Buffer A was then performed. For the MBP-R. denitrificans GapR protein that was to be used for Mass Photometry experiments two extra wash steps were included before elution to ensure contamininating DNA was removed. First one column volume of 50 mM Tris-HCl pH 7.5, 1.5 M NaCl, 5% (v/v) glycerol, 5 mM $MgCl_2$, 0.5 mM βME was used. Then one column volume of 50 mM Tris-HCl pH 7.5, 1.5 M NaCl, 5% (v/v) glycerol, 5 mM $MgCl_2$, 0.5 mM βME with 2 M Urea

was added as a wash. These two extra washes were followed by another colum volume wash of Buffer A before elution. The proteins were eluted in Buffer A in an increasing gradient of imidazole. Fractions were analyzed by SDS-PAGE and those containing the protein were combined. Proteins were typically 90% pure at this stage. The fractions were then concentrated using Sigma-Millipore concentrators (Amicon). Proteins used in crystallization trails were subjected to a second purification step using size exclusion chromatography (SEC) on a Superdex75 pg column and an ÄKTA prime plus. The buffer used for this step was 25 mM Tris-HCl pH 7.5, 150 mM NaCl, 5% (v/v) glycerol, 5 mM $MgCl_2$ and 0.5 mM βME. His-tags were removed by thrombin digestion overnight at room temperature (rt) using a thrombin cleavage capture kit (EMD Millipore; Catalog #69022). Cleaved His-tags were removed by loading the cleavage reactions onto Ni-NTA columns and collecting the flow through. The proteins were concentrated using centricons (Amicon) with a 10 kDa MW cutoff.

Selenomethionine substituted RDJLΦ1 phage GapR was generated using the methionine inhibitory pathway. For these cell growths, a 500 mL overnight culture of LB with 0.10 mg/mL ampicillin was first inoculated with a colony of the C41(DE3) cells containing the expression vector. The next day the cells were spun and the supernatant discarded and resuspended in 50 mL of 1X M9 media with 0.10 mg/mL ampicillin. The cells were spun and resuspended again (to ensure removal of LB). A final spin and resuspension of the cells in 1 X M9 media was done and these cells inoculated into 9 liters of 1X M9 media with 0.10 mg/mL ampicillin (and 2 mM $MgSO_4$, 2.5% (w/v) dextrose, 5 mM $CaCl_2$) and grown at 37 °C to an OD_{600} of 0.25-0.30. Then inhibitory amino acids (100 mg/L of lysine,

phenylalanine and threonine, 50 mg/L of isoleucine, leucine and valine and 100 mg/L selenomethionine) were added, the temperature reduced to 15 °C and the cells grown for 20 min. 1 mM IPTG was then added and the cells grown overnight. The next day the cells were spun and the selenomethionine protein was purified as per the WT except that 1.0 mM βME was included in the buffers.

Crystallization and structure determination of RDJLΦ1 GapR and Roseobacterial GapR crystals

For crystallization trials RDJLΦ1 phage GapR, *R. denitrificans* GapR and *Roseobacterial* MED193 sp. GapR were concentrated to 30 mg/mL, 20 mg/mL and 20 mg/mL, respectively. For crystallization screens of the *R. denitrificans* GapR with DNA, the protein, at 20 mg/mL, was mixed at a ratio of 4:1 (protein subunit: dsDNA) with AT-rich dsDNA sites ranging from 12 bp to 20 bp. Wizard screens I to IV, Natrix and Natrix 2, and cryo I and II were used for screening these proteins and complexes at rt by the hanging drop vapor diffusion method. The best diffracting RDJLΦ1 GapR crystals were produced by mixing the protein 1:1 with a crystallization solution consisting of 20% (w/v) PEG 3350, 0.2 M ammonium citrate dibasic. A second RDJLΦ1 GapR crystal form was grown by mixing the protein 1:1 with a crystallization reagent consisting of 50 mM sodium cacodylate pH 6.0, 2 mM $CaCl_2$, 1.8 M ammonium sulphate, 0.5 mM spermine. Both crystals were cryo-preserved by dipping them for 1-2 s in 2 μL of the crystallization solution supplemented with 15%-20% (v/v) glycerol before plunging into liquid nitrogen. Roseobacterial MED193 sp. GapR crystals were grown by mixing the protein solution 1:1 with a crystallization solution consisting of 0.1 M 4-(2-hydroxyethyl)piperazin-1-

yl]ethanesulfonic acid (HEPES) pH 7.5 and 25% (w/v) PEG 6000. The crystals were cryo-preserved by dipping them for 1-2 s in 2 μL of the crystallization solution supplemented with 15% (v/v) glycerol before plunging into liquid nitrogen. Crystals of the *R.denitrificans* GapR in complex with a 18mer self complementary dsDNA site (5'-TTATTAATTAATTAATAA-3'), were obtained by mixing the protein-DNA complex 1:1 with a crystallization reagent composed of 25% (v/v) PEG 400, 0.1 M *N*-cyclohexyl-2-aminoethanesulfonic acid (CHES) pH 9.5. The crystals could be cryo-preserved straight from the drop.

The RDJLΦ1 phage GapR crystals could not be solved by Molecular Replacement (MR)[35] using previous GapR structures or predicted models available at that time. Hence, for phasing, Semet RDJLΦ1 GapR was generated and used to produce crystals. Single wavelength anomalous diffraction (SAD) data were collected at the Se edge at ALS beamline 5.0.2 and the data processed with XDS[36] (version January 10, 2022). Phenix Autosol[35] (Version 1.20.1-4487-000) was used to find selenium sites. Autosol was then used to optimize heavy atom parameters and perform density modification[35]. The experimental map was of excellent quality and allowed the model to be readily fit and then refined in Phenix_refine. There is one subunit in the crystallographic asymmetric unit (ASU) and the dimer is generated by symmetry. See Table S1 for final data collection and refinement statistics. Data for the second crystal form of RDJLΦ1 GapR were collected at ALS beamline 5.0.2 and MR was used to solve the structure, with our RDJLΦ1 GapR structure solved by SAD as a search model. Two solutions were found and revealed the

same dimer as observed in the first crystal form. See Table S1 for data collection and refinement statistics.

Data for the apo Roseobacterial MED193 sp. GapR crystals were obtained at ALS BL 5.0.2 and processed with XDS[36]. The structure was solved by MR using the GapR structure (pdb code: 6CFY) as a search model. After fitting the Roseobacteria*l* GapR sequence into the model using Coot[37], Phenix was used for refinement35. Data for the *R. denitrificans* GapR-DNA complex were collected at ALS beamline 5.0.3 and processed with XDS[36]. The structure was solved by MR using a subunit of the 6CG8 structure as a search model. One solution was found (the dimer-of-dimers is generated by crystallographic symmetry) and the structure refined in Phenix. After a round of refinement, the *C. crescentus* residues were replaced with the *R. dentrificans* protein and final refinement carried out, with waters added at the last step. Notably, though the crystals could not be obtained without DNA, there was no density for the DNA in the electron density maps. Hence, to obtain an unbiased phases, we soaked crystals with 1 mM $HgCl_2$ for two days and collected data on our in house XtaLab Synergy diffractometer, which is equipped with a Cu PhotoJet x-ray generator, HyPix-6000HE detector, and 800 Series Cryostream Cooler. Data scaling was performed using CrysAlis^{Pro}. X-ray intensity data were merged using Aimless. The data was scaled to a high resolution cutoff of 2.90 Å. The R_{merge} was 5.8% (highest shell was 32.1%), R_{pim} was 1.4% (7.6%), the I/σI was 50 (10.8), the CC(1/2) was 1.00 (0.996) and the redundancy was 33 (35). Phenix Autsol was used to determine a SAD solution and resulted in a Figure of Merit of 0.37 and a Bayes-

CC of 42.7. The SAD map revealed clear density for the protein but no clear density for the DNA supporting that the DNA was not ordered in the structure.

Confocal microscopy

eGFP superfolder-Roseobacterial GapR and mCherry-tagged RDJLΦ1 GapR were produced as codon optimized (for *E. coli* expression) genes and subcloned into pET15b. In these constructs the eGFP and mCherry proteins were expressed at the N-terminus of the protein and linked via GGSGGSGGS sequence to the Roseobacterial and phage GapRs, respectively. A coexpression construct was also generated by subcloning the two genes into pETDuet-1. C41(DE3) cells were transformed with the plasmids and colonies expressing the transformants were grown in 2 mL of LB medium supplemented with ampicillin at 100 mg/mL overnight at 37 °C with shaking at 200 rpm. One milliliter of induction culture was then made by combining 100 mL of the overnight culture with 0.9 mL of LB medium with the antibiotic plus 1.0 mM IPTG. After induction for 3 h at 37°C with shaking at the same speed, the cells were placed on 1.2% agarose LB pads, and sealed using a gene frame and a coverslip and analysed. eGFP-Roseobacterial GapR localization was imaged by excitation at 488 nm and absorption at 509 nm, mCherry-phage GapR was imaged by excitation at 561 nm and absorption at 600 nm. To localize DNA, the cells were stained with DAPI for 5 min at rt (the staining mixture was made by combining 250 mL of the induced cells and 1.0 mL of the 1 mg/μL DAPI solution), and prepared as for the other samples. Confocal microscopy was performed using an inverted Zeiss 780 laser-scanning confocal microscope.

Size exclusion chromatography (SEC)

RDJLΦ1 GapR and the RDJLΦ1GapR(I24E-I27E) mutant were purified as described and exchanged into a buffer composed of 25 mM Tris, pH 7.5, 5% (v/v) glycerol, 0.5 mM βME, 150 mM NaCl., 5 mM $MgCl_2$. The proteins were concentrated to 0.7 mg/mL (70 μM) and injected over a HiLoad 26/600 Superdex 75 pg column equilibrated in the protein buffer. Protein elutions were monitored by intrinsic UV-absorbance. The protein molecular weights were determined using a gel phase distribution coefficient calibration curve (K_{av} = $[V_e - V_0]/[V_C - V_0]$). The void volume, V_0, was determined using Blue Dextran (~2000 kDa) and the column's accessible volume, V_C, is given by 320 mL. Elution volumes, V_e, were determined for four protein standards: aprotinin, ~6.5 kDa; cytochrome c, ~12.4 kDa; carbonic anhydrase, 29 kDa.

Mass Photometry (MP) experiments

MP experiments (38) were done using a Refeyn TwoMP instrument (Oxford, UK). The experiments were performed using microscope coverslips, cleaned by sequential sonication in isopropanol (HPLC grade, and Milli-Q H2O (15 min each)), followed by drying with a clean, pressurized air stream. Clean coverslips were assembled into the flow chamber, and silicone gaskets were positioned on the glass surface for sample loading to hold the sample drops with 4 × 4 wells prior to measurements. Contrast-to-mass calibration was achieved by measuring the contrast of proteins in the native marker protein standard mixture (NativeMark Protein Standard, Thermo Fisher Scientific) to generate a standard calibration curve; 1048 kDa, 480 kDa, 146 kDa, and 66 kDa Molecular masses were used to fit the calibration curve with an R2 value of 0.998 and a

Max mass error of 11.3% in the Refeyn DiscoverMP v2023 R2 software. Calibration was applied to each sample measurement to calculate the molecular mass of each histogram distribution during analysis.

Glutaraldehyde crosslinking

Glutaraldehyde crosslinking experiments were carried out on WT phage GapR and RDJLΦ1GapR(I24E-I27E) proteins at 0.4 mg/mL in a buffer composed of 25 mM 2-(N-morpholino)ethanesulfonic acid (MES) pH 6.5, 125 mM NaCl. For the reactions, glutaraldehyde was added to a final concentration of 0.05% (w/v) and the reaction was run for 15 min. SDS running buffer was then added 1:1 and the samples immediately boiled for 2 min prior to running on SDS gels.

Fluorescence polarization (FP) binding experiments

To measure DNA binding by RDJLΦ1 GapR, *R. denitrificans* GapR, *R. denitrificans* GapR(K46D-R54D-K68D), 1:1 mixture of RDJLΦ1 GapR-*R. denitrificans* GapR and the RDJLΦ1 GapR-*R. denitrificans* GapR chimera, the fluoresceinated 20mer DNA (top strand: 5´-ATTATTAATTAATTAATAAT-3´) was used. In each experiment, increasing concentrations of the GapR protein was titrated into the sample cell containing 1 nM of the DNA in a buffer of 25 mM Tris-HCl pH 7.5, 125 mM NaCl, 2.5% (v/v) glycerol. FP experiments investigating RDJLΦ1 GapR and *R. denitrificans* GapR binding to the fluoresceinated GC-rich site (top strand: 5´-CGCGCCGGCCGGCCGGCGCG-3´) were also performed. Samples were excited at 490 nM and fluorescence emission was measured at 530 nM. The resultant data were plotted using KaleidaGraph version 4.5 for

Mac; serial #8011073 (Synergy software) and the curves fit with single site binding mode. Three technical repeats were performed for each curve and the standard errors from the three affinities were determined.

Bacterial two-hybrid plasmid construction and analysis

Constructs for B2H assays were PCR amplified from genomic DNA or gBlocks using KOD DNA polymerase. PCR products were then digested using KpnI-HF and XbaI (New England Biolabs) and ligated into pUT18, pUT18C, pKT25, or pKNT25 digested with the same enzymes. Ligated plasmids were then transformed into DH5α *E. coli* and validated by sanger sequencing. Plasmids (pUT18, pUT18C, pKT25, and pKNT25) containing fusion constructs of GapR variants were co-transformed into the two-hybrid assay strain BTH101.

For two-hybrid experiments, four replicates from each transformation were picked, grown in supplemented M63 minimal media for 48 h, and spotted on MacConkey agar plates supplemented with carbenicillin, kanamycin, 1% (w/v) maltose, and 1mM IPTG. Plates were incubated at 30 °C and imaged after 72 h. Interactions were probed fully in two orientations including C-terminal fusions and N-terminal fusions (e.g., T25-JessA GapR with T18-JessA GapR, and the inverse), with some interactions being tested with cross-oriented tags (e.g., JessA GapR-T18 with T25-JessA GapR) for verification of phenotypes.

ACKNOWLEDGEMENTS

We acknowledge beamline 5.0.2 for X-ray diffraction data collection. The ALS (Berkeley, CA) is a national user facility operated by Lawrence Berkeley National Laboratory on behalf of the US Department of Energy under Contract DE-AC02-05CH11231, Office of Basic Energy Sciences. Beamline 5.0.2 of the ALS, a US Department of Energy Office of Science User Facility under Contract DE-AC02-05CH11231, is supported in part by the ALS-ENABLE program funded by the NIH, National Institute of General Medical Sciences, Grant P30 GM124169-01.

DATA AVAILABILITY

The atomic coordinates and structure factor amplitudes for the structures have been deposited in the Protein Data Bank (https://www.rcsb.org) and are publicly available as of the date of publication. Accession codes are 10OK,10ON,10OS and 10PH.

Any additional information required to reanalyse the data reported in the paper is available from the corresponding author upon request.

SUPPLEMENTARY DATA

Supplementary data are available at NAR online.

FUNDING

Nanaline H Duke Endowed Chair and National Institutes of Health [R35GM130290 and R01AI154524 to M.A.S., R35GM154727 and R00GM134153 to M.S.G.].

CONFLICTS OF INTEREST STATEMENT

None declared.

REFERENCES

1. Cunha, S. Woldrich, C.L. & Odijk, T. (2001). Polymer-mediated compaction and internal dynamics of isolated *Escherichia coli* nucleoids. *J. Struct. Biol.* **136**, 53-66.

2. de Vries, R., (2010). DNA condensation in bacteria: interplay between macromolecular crowding and nucleoid proteins. *Biochimie* **92**, 1715-1721.

3. Joyeux, M. (2010). Compaction of bacterial genomic DNA: clarifying the concepts. *J. Phys. Condens. Matter* **27**, Article 38301.

4. Dame, R.T. (2005). The role of nucleoid-associated proteins in organization and compaction of bacterial chromatin. *Mol. Microbiol*. **56**, 858-870.

5. Holowka, J. & Zakrzewska-Czerwinska, J. (2020). Nucleoid associated proteins: the small organizers that help to cope with stress. *Front. Microbiol.* **11**, 10.3389.

6. Rimsky, S. & Travers, A. (2011). Pervasive regulation of nucleoid structure and function by nucleoid-associated proteins. *Curr. Opin. Microbiol.* **14**, 136-141.

7. Wang, X., Llopis, P.M. & Rudner, D.Z. (2013). Organization and segregation of bacterial chromosomes. *Nat. Rev. Genet*. **14**, 191-203.

8. Luijsterburg, M.S., White, M.F., van Driel, R. & Dame, R.T. (2008). The major architects of chromatin. Architectural proteins in bacteria, archaea and eukaryotes. *Crit. Rev. Biochem. Mol. Biol.* **43**, 393–418.

9. Dillon, S.C. & Dorman, C.J. (2010). Bacterial nucleoid-associated proteins, nucleoid structure and gene expression. *Nat. Rev. Microbiol*. **8**, 185–195.

10. Ricci, D.P., Melfi, M.D., Lasker, K. & Shapiro, L. Cell cycle progression in *Caulobacter* requires a nucleoid-associated protein with high AT sequence recognition. *Proc. Natl. Acad. Sci. USA* E5952-E5961 (2016).

11. Arias-Cartin, R. *et al.* Replication fork passage drives asymmetric dynamics of a critical nucleoid-associated protein in *Caulobacter. EMBO J.* **23**, 301-318 (2016).

12. Taylor, J.A., Pansi, G., Viollier, P.H. & Marczynski, G.T. A novel nucleoid-associated protein coordinates chromosome replication and chromosome partition. Nucleic Acids Res. **45**, 8916-8929 (2017).

13. Guo, M.S., Haakonsen, D.L., Zeng, W., Schumacher, M.A. & Laub, M.T., (2018). A bacterial chromosome structuring proteins binds overtwisted DNA to stimulate type II topoisomerases and enable DNA replication. *Cell* **175**, 583-597.

14. Huang, Q., Duan, B., Cong, X., Fan, S. & Xia, B. GapR binds DNA through dynamic opening of its tetramer interface. *Nucleic Acids Res.* **48**, 9372-9386 (2020).

15. Tarry, M.J., Harmel, C., Taylor, J.A., Marczynski, G.T. & Schmeing, T.M. Structures of GapR reveal a central channel which could accommodate B-DNA. *Sci. Rep*. **9**, 16679 (2019).

16. Lourenco, R.F., Saurabh, S., Herrmann, J., Watasuki, S. & Shapiro, L. The nucleoid-associated protein GapR uses conserved structural elements to oligomerize and bind DNA. *mBio* **11**, e00448-20 (2020).

17. Guo, M.S., Kawamura, R., Littlehale, M.L., Marko, J.F. & Laub, M.T. High-resolution, genome-wide mapping of positive supercoiling in chromosomes. *eLife* **10**, e67236 (2021).

18. Fu, Z., Guo, M.S., Zhou, W. & Xiao, J. Differential roles of positive and negative supercoiling in organizing the *E. coli* genome. *Nucleic Acids Res*. **25**, 724-737 (2024).

19. Cockrell, A.J. *et al.* Regulators of rDNA array morphology in fission yeast. *PLoS Genet.* **5**, e1011331 (2024).

20. Gupta, R.S. & Mok, A. Phylogenomics and signature proteins for the alpha Proteobacteria and its main groups. *BMC Microbiol*.**7**, 10.1186 (2007).

21. Flores-Rios, R., Quatrini, R. & Loyola, A. Endogenous and foreign nucleoid-associated proteins of bacteria: occurrence, interactions and effects on mobile genetic elements and host's biology. *Comput. & Struct. Biotech*. **17**, 746-7566 (2019).

22. Son, B. *et al*. A phage-encoded nucleoid associated protein compacts both host and phage DNA and depressed H-NS silencing. *Nucleic Acids Res.* **49**, 9229-9245 (2021).

23. Ben Bdira, F*. et al.* Novel anti-repression mechanism of H-NS proteins by a phage protein. *Nucleic Acids Res.* **49**, 10770-10784 (2021).

24.Ali, S.S., Beckett, E., Bae S.J. & Navarre, W.W. The 5.5 protein of phage T7 inhibits H-NS through interactions with the central oligomerization domain. *J. Bacteriol.* **193**, 4881–4892 (2011).

25.Ho, C.H., Wang, H.C., Ko, T.P., Chang, Y.C. & Wang, A.H. The T4 phage DNA mimic protein Arn inhibits the DNA binding activity of the bacterial histone-like protein H-NS. *J. Biol. Chem.* **289**, 27046–27054 (2014).

26. Liu, Q. & Richardson, C.C. Gene 5.5 protein of bacteriophage T7 inhibits the nucleoid protein H-NS of *Escherichia coli. Proc. Natl. Acad. Sci. USA* **90**,1761–1765 (1993).

27. Zhang, P., Zhao, X., Wang, Y. & Liu, B. Bacteriophage protein Gp46 is a cross-species inhibitor of nucleoid-associated proteins. *Proc. Natl. Acad. Sci. USA* **119**, e211627819 (2022).

28. Chakraborti, S. *et al.* A bacteriophage mimic of the bacterial nucleoid-associated protein Fis. *Biochem. J*. **477**, 1345-1362 (2020).

29. Bdira, F.B. *et al*. Novel anti-repression mechanism of H-NS proteins by a phage protein. *Nucleic Acids Res.* **49**, 10770-10784 (2021).

30. Luo, H. & Moran, M.A. Evolutionary ecology of the marine Roseobacter clade. *Microbiol. Mol. Biol. Rev.* **78**, 573-587 (2014).

31. Buchan, A., Gonzalez, J.M. & Moran, M.A. Discoveries with Roseobacteraceae: bacterial models for ocean heterotrophy. *Annu. Rev. Marine Sci.* **18**, 15:44 (2025).

32. Simon, M. *et al.* Phylogenomics of Rhodobacteraceae reveals evolutionary adaptation to marine and non-marine habitats. *ISME J*. **11**, 1482-1499 (2017).

33. Zhang, Y. & Jiao, N. A roseophage RDJLΦ1, infecting the aerobic anoxygenic phototropic bacterium *Roseobacter denitrificans* OCh114. *Appl. Env. Microbiol.* **75**, 1745-1749 (2009).

34. Huang, S., Zhang, Y., Chen, F. & Jiao, N. Complete genome sequence of a marine roseophage provides evidence into the evolution of gene transfer agents. *Virol. J.* **8**, 124 (2011).

35. Liebschner, D. *et al.* Macromolecular structure determination using X rays, neutrons and electrons: Recent developments in Phenix. *Acta Crystallogr. D Struct. Biol.* **75**, 861 877 (2019).

36. Kabsch, W. (2010). XDS. *Acta Cryst.* **D66**, 125-132 (2019).

37. Emsley, P., Lohkamp, B., Scott, W.G. & Cowtan, K. Features and Development of Coot. *Acta Cryst.* **D66**, 486-501 (2010).

38. Young, G. *et al.* Quantitative mass imaging of single biological macromolecules. *Science* **360**, 423-427 (2018).

39. Schumacher, M.A., Singh, R.R. & Salinas, R. Structural studies on the *M. tuberculosis* nucleoid associated protein, NapA, indicates DNA bridging mechanism. *J. Mol. Biol*. **437**, 169486 (2025).

40. Duan, X., Hall, J.A., Nikaido, H. & Quiocho, F.A. Crystal structures of the maltodextrin/maltose-binding protein complexes with reduced oligosaccharides: flexibility of tertiary structure and ligand binding*. J. Mol. Biol.* **306**, 1115-1126 (2001).

41. Karimova, G., Pidoux, J., Ullmann, A. & Ladant, D. A bacterial two-hybrid system based on a reconstituted signal transduction pathway. *Proc. Natl. Acad. Sci. USA* **95**, 5752–5756 (1998).

42. Pina-Iturbe, A. *et al*. Horizontally acquired homologs of Xenogeneic Silences: Modulators of gene expression encoded by plasmids, phages and genomic islands. *Genes*, **11**, 10.3390 (2020).

43. Adams, M.C. *et al.* The crystal structure of bacteriophage λ RexA protein provides novel insights into the DNA binding properties of Rex-like phage exclusion proteins. *Nucleic Acids Res*. **52**, 4659-4675 (2024).

44. Kumaramswami, M., Howe, M.M. & Park, H-W. Crystal structure of the Mor protein of bacteriophage Mu, a member of the Mor/C family of transcription activators. *J. Biol. Chem.* **279,** 16581-16590 (2004).

45. Williamson, H.S. & Free, A. A truncated H-NS-like protein from enteropathogenic *Escherichia coli* acts as an H-NS antagonist. *Mol. Microbiol.* **55**, 808–827 (2005).

46. Müller, C.M. *et al.* Differential effects and interactions of endogenous and horizontally acquired H-NS-like proteins in pathogenic *Escherichia coli*. *Mol. Microbiol.* **75**, 280–293 (2010).

47. Mellies, J.L. *et al.* Ler of pathogenic *Escherichia coli* forms toroidal protein-DNA complexes. *Microbiology* **157**, 1123–1133 (2011).

48. Yun, C.-S. *et al.* Pmr, a histone-like protein H1 (H-NS) family protein encoded by the IncP-7 plasmid pCAR1, is a key global regulator that alters host function. *J. Bacteriol.* **192**, 4720–4731 (2010).

49. Lang, K.S. & Johnson, T.J. Characterization of Acr2, an H-NS-like protein encoded on A/C2-type plasmids. *Plasmid* **87-88**, 17–27 (2016).

50. Zhan, Y. & Chen, F. Bacteriophages that infect marine roseobacters: genomics and ecology. *Environ. Microbiol*. **21**, 1885-1895 (2019).

51. Liang, Y. *et al.* Complete genome sequence of the siphovirus Roseophage RDJLΦ2 infecting *Roseobacter denitrificans* Och114. *Marine Genomics* **25**, 17-19 (2016).

52. The PyMOL Molecular Graphics System, Version 2.55. Schrödinger, LLC.

Figure Legends

Figure 1. **Multiple sequence alignment (MSA) of bacrterial and phage GapRs**. MSA of select GapRs from α-proteobacteria (lettering in black), α-proteobacterial phages (lettering in light blue) and roseophages of the *Siphoviridae* class (lettering in red). Conserved residues in all sequences are indicated by asterisks under the sequence and moderately conserved residues by inverted arrows. Residues involved in DNA binding revealed in previous GapR crystal structures are highlighted in limon and the N-cap

residue in bacterial GapRs is highlighted in yellow. Above the sequences are the secondary structural elements as determined from the DNA bound form of the *C. crescentus* GapR and the apo RDJLΦ1 phage GapR. In apo bacterial GapRs, α2 and α3 form a single long helix. The GapR proteins are from the following bacteria: *Caulobacter crescentus*, *Bosea* Root 381, *R. denitrificans, Roseobacter* MED193, *Roseobacter* sp. OBYS, *Pseudophaeobacter* sp., *Ruegeria* sp. NA, *Sedimentitalea* sp., *R. adriaticum*, *A. haliotis*, *R. bhavnagarense*, *F. mediterranea*, *R. halophilus, Paracoccaceae*, *P. flagellates;* α-proteobacterial phages*: Caulobacter* phage Cr30 phage, Bacteriophage sp. from QHJ82727.1 MAG*, Ochrobacterium* phage POA26, *Rhizobium* phage RL2RES, *Rhizobium* phage RHph_I1_9, *Sinorhizobium* phage ΦM9, *Ruegeria* phage vB RpoS-V16, *Agrobacterium* phage 7-7-1, *Synechococcus* virus S-ESS1, *Rhizobium* phage vB RleM P10VF; *Siphoviridae* class Rosephages: RDJLΦ1, RDJLΦ2,. RDJL6, RDCBΦ1.

Figure 2. Structure of the RDJLΦ1 roseophage GapR protein. **A** Section of the selenomethionine SAD experimental map (blue mesh) contoured at 1 σ. Shown within the map is the final structure, which is dimeric. One subunit is colored magenta and the other is limon. **B** Overall cartoon diagram of the RDJLΦ1 GapR dimer, with each subunit colored as in Figure 2A. The secondary structural elements are labeled. **C** Close up, colored as in Figure 2A, of the coiled coil dimer interface formed between the two-related α1 helices of the structure. Shown as sticks are key residues that mediate dimerization. **D** Close up of the helical dimer interaction formed at each end of the dimer between α1

and α2'-α3' of the other subunit. The interface is hydrophobic and shown as sticks are residues within the interface. All cartoon figure depictions were made using PyMOL[52].

Figure 3. Comparison of the RDJLΦ1 GapR structure to the two conformations of bacterial GapRs. RDJLΦ1 GapR is a dimer with one subunit colored limon and the other magenta. The apo bacterial GapR is colored similarly. Note, all the structures share a common α1-α1' dimer. In the DNA bound form of GapR (6CG8) (right) one dimer is colored similar to the RDJLΦ1 and apo bacterial GapRs and the other subunits are colored white to allow comparison of the colored dimers which are shown in the same orientations. Notably, while the RDJLΦ1 GapR structure contains an α3 of similar length to that of the bacterial DNA bound form, the α3s are oriented entirely differently. Notably, though the RDJLΦ1 α3 is positioned similarly to α3 of another subunit on the formed dimer-of-dimers in the DNA bound bacterial GapR (as indicated by a dashed box). This suggests that the phage GapR would be prevented from forming the dimer-of-dimer state and hence DNA binding.

Figure 4. RDJLΦ1 GapR has a different structure from the bacterial GapRs. **A** Overlay of the two distinct crystal structures of RDJLΦ1 GapR, one colored magenta and the other yellow. Both structures reveal the same dimerization mode. **B** Close up of the region containing the α1-α2 turn and the α2-α3 turn in the RDJLΦ1 GapR structure. G42 forms the turn between α1 and α2 in the RDJLΦ1 GapR and is one of the few residues conserved among all GapRs. The hydrophobic residue located in the turn facilitates packing of the α3 helix with α2 and α1' helices. **C** Close up of the region analogous to

Figure 3B in the *Caulobacter* GapR-DNA complex. G52 corresponds to G42 in the phage GapR. DNA binding in the bacterial GapR also induces structural changes leading to breaking α2 into α2 and α3. Here the Asp residue in the middle of the apo α2 helix breaks the helix at this point and serves as a N-cap residue to stabilize the newly formed α3. The α2-α3 turn is thus shorter in the bacterial GapR structures compared to the RDJLΦ1 GapR. **D** Close up of the region analogous to Figure 3B-C in the apo form of the Caulobacter GapR structure. Here each subunit only has two helices, with the N-cap forming aspartic acid being part of the extended α2. **E** Comparison of the amino acid sequences of the RDJLΦ1 GapR α2-α3 region with the Caulobacter sequence. Above the alignment is the secondary structural elements present in the structures, underscoring that the RDJLΦ1 GapR structure has a longer loop between α2 and 3 and that in the bacterial GapR structure, this region forms a long uninterrupted helix, which undergoes a conformational changes upon DNA binding leading to two helices. **F** Overlay of the α1 helices of the RDJLΦ1 GapR dimer (magenta) onto the corresponding helices in the *C. crescentus* GapR-DNA structure (tan). Strikingly, the α3 helices of the RDJLΦ1 GapR superimpose onto the α3 helices (grey) from the *C. crescentus* GapR subunits from the other dimer. This overlay indicates that the RDJLΦ1 GapR dimer could not form the same DNA induced dimer-of-dimers observed in the bacterial GapR structures.

Figure 5. Biochemical characterization of the RDJLΦ1 GapR and test of the structural model. **A** Size exclusion chromatography (SEC) of the RDJLΦ1 GapR. Left is the elution profile and to the right is the plot of the Log MW and column volume (x and y axes, respectively). RDJLΦ1 GapR eluted at a calculated MW of 28 kDa (blue circle),

consistent with a dimer. The standards used for calculation of the standard curve are shown as dark green circles and were cytochrome c oxidase (12.4 kDa), carbonic anhydrase (29 kDa), and albumin (66 kDa). **B** Mass photometry (MP) of the RDJLΦ1 GapR at 25 nM. For these experiments the protein was diluted immediately from 100 μM to 25 nM and then analyzed. **C** Same protein sample as in Figure 5B but here the samples were analyzed after diluting from 100 μM to 25 nM and incubating the sample overnight at 4 ºC. Both experiments in **B** and **C** were done in the absence (black plot) and presence (blue plot) of 150 nM 20mer AT-rich DNA.

Figure 6. Structures of the roseobacterial GapR and DNA binding. **A** Structure of the apo Rosepbacterial GapR with helices labeled. One subunit is colored magenta and one is limon. Also indicated are hydrophobic residues involved in the α1-α1' interface. **B** Structure of the roseobacterial GapR solved complexed with DNA. Note the density for the DNA was not evident in the structure. However, the structure revealed the dimer-of-dimers/tetramer form previously visualized bound to DNA for the *C. crescentus* GapR. **C** Structure in **B** shown with modeled DNA where the DNA is shown as a grey surface. **D** FP studies of *R. dentrificans* GapR, *R. dentrificans* GapR(K46D-R54D-K68D) and RDJLΦ1 GapR binding to the fluoresceintly tagged DNA duplex (top strand: 5´-ATTATTAATTAATTAATAAT-3´). *R. dentrificans* GapR bound with a K_d of 150 ± 25 nM while RDJLΦ1 GapR and *R. dentrificans* GapR(K46D-R54D-K68D) showed no detectable binding. The *x* and *y* axes are concentration of each GapR protein in nM and millipolarization units, respectively. Three technical repeats were performed for each

(shown is a representative binding curve) and the standard errors from the three affinities were determined.

Figure 7. Confocal microscopy of roseobacterial and RDJLΦ1 GapR proteins. **A** Confocal microscopy examining the cellular localization of expressed eGFP-labeled roseobacterial GapR in *E. coli.* Left shows nucleoid labeling with DAPI, center is the eGFP label analyses and right is the merge of the two images. **B** Confocal microscopy examining the cellular localization of expressed mCherry-labeled RDJLΦ1 GapR in *E. coli.* Left shows nucleoid labeling with DAPI, center is the mCherry label analyses and right is the merge of the two images. **C** Confocal microscopy examining the cellular localization of E. coli containing coexpressed eGFP-roseobacterial GapR and mCherry-lRDJLΦ1 GapR. Left shows nucleoid labeling with DAPI, center is the mCherry, eGFP label analyses and right are merges of mCherry with eGFP, mCherry with DAPI and eGFP with DAPI.

Figure 8. RDJLΦ1 GapR interacts with roseobacterial GapR. **A** Model of the RDJLΦ1 GapR (limon) dimerized with the roseobacterial GapR (magenta). Note, this modeling shows there are no clashes that would prevent heterodimerization. **B** MP data analyses of MNP-*R. dentrificans* GapR at concentration of 25, 50, 100 and 200 nM after 1 h incubation at rt. **C** Left, schematic of the bacterial two-hybrid (B2H) assay. **D** B2H results for *Roseobacter* and RDJLΦ1 GapR interactions. **E** B2H results for *Roseobacter* or RDJLΦ1 GapR interactions with *Caulobacter* GapR and Caulobacter phage Cr30, JessA, and RW GapR. **F** FP studies of *R. dentrificans* GapR (blue), RDJLΦ1 GapR-

roseobacterial GapR 1:1 mixture (green) and the RDJLΦ1 GapR-roseobacterial GapR complex produced from the chimera. Binding to the fluoresceintly tagged DNA duplex (top strand: 5´-ATTATTAATTAATTAATAAT-3´) was analyzed. *R. dentrificans* GapR bound with a K_d of 150 ± 25 nM while RDJLΦ1 GapR and *R. dentrificans* GapR(K46D-R54D-K68D) showed weak but non saturable binding. The *x* and *y* axes are concentration of each GapR protein in nM and millipolarization units, respectively. Three technical repeats were performed for each (shown is a representative binding curve) and the standard errors from the three affinities were determined.

Figure 9. Schematic mechanism of RDJLΦ1 GapR as a poison for roseobacterial GapR DNA binding. Right shows the structure of the R. denitrificans GapR that exists in an equilibrium between monomer and oligomer states. DNA binding stabilizes the dimer-of-dimer DNA state. Left shows the RDJLΦ1 GapR existing in the cytosol in an equilibrium between monomer and dimer states. Formation of the RDJLΦ1-*Roseobacter* heterodimer creates an inactivated state as the location of the phage α3 prevents formation of a DNA binding clamp.

Figure 1

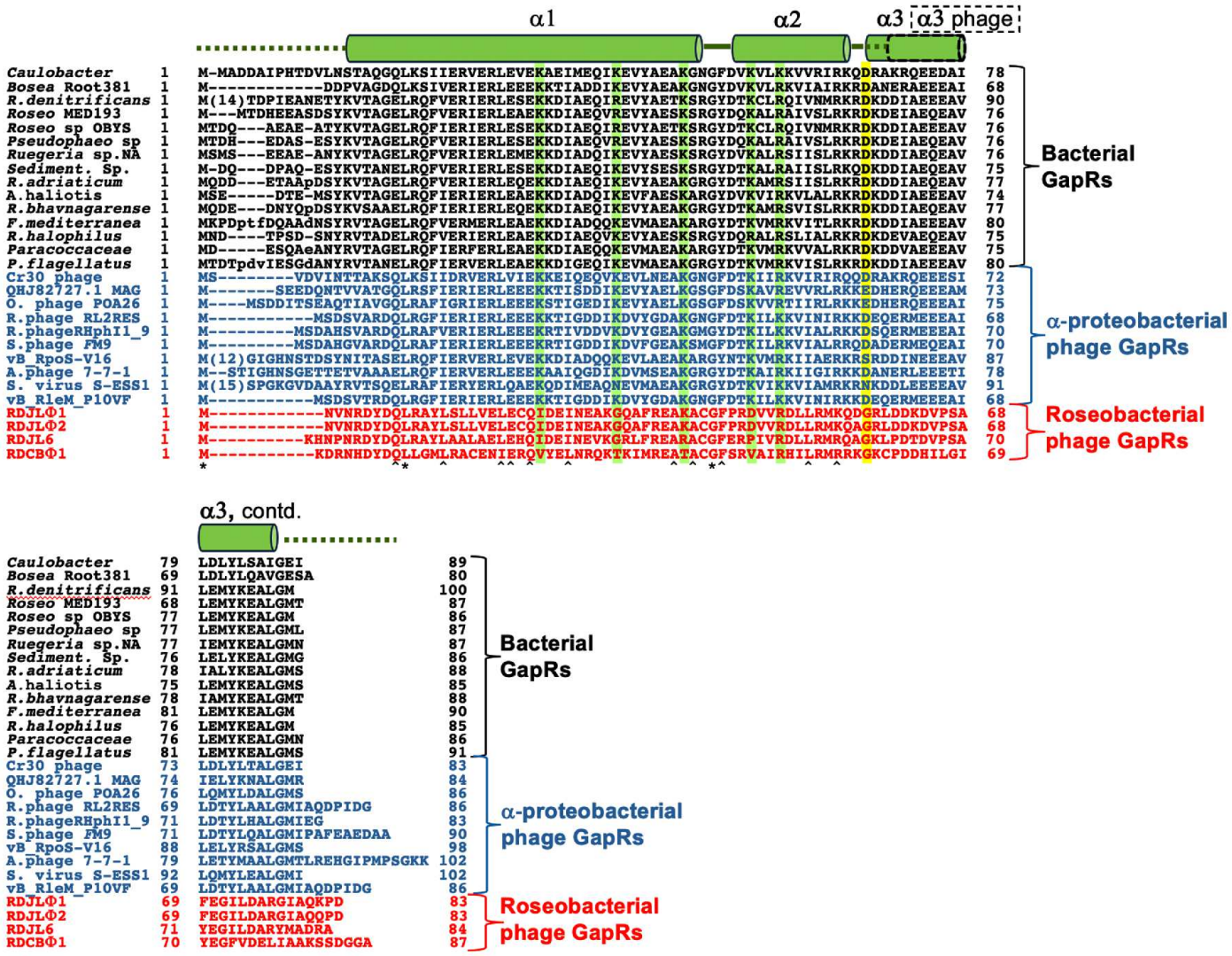
α1
α2
α3
α3 phage
Bacterial GapRs
α-proteobacterial phage GapRs
Roseobacterial phage GapRs
α3, contd.
Bacterial GapRs
α-proteobacterial phage GapRs
Roseobacterial phage GapRs

Figure 2

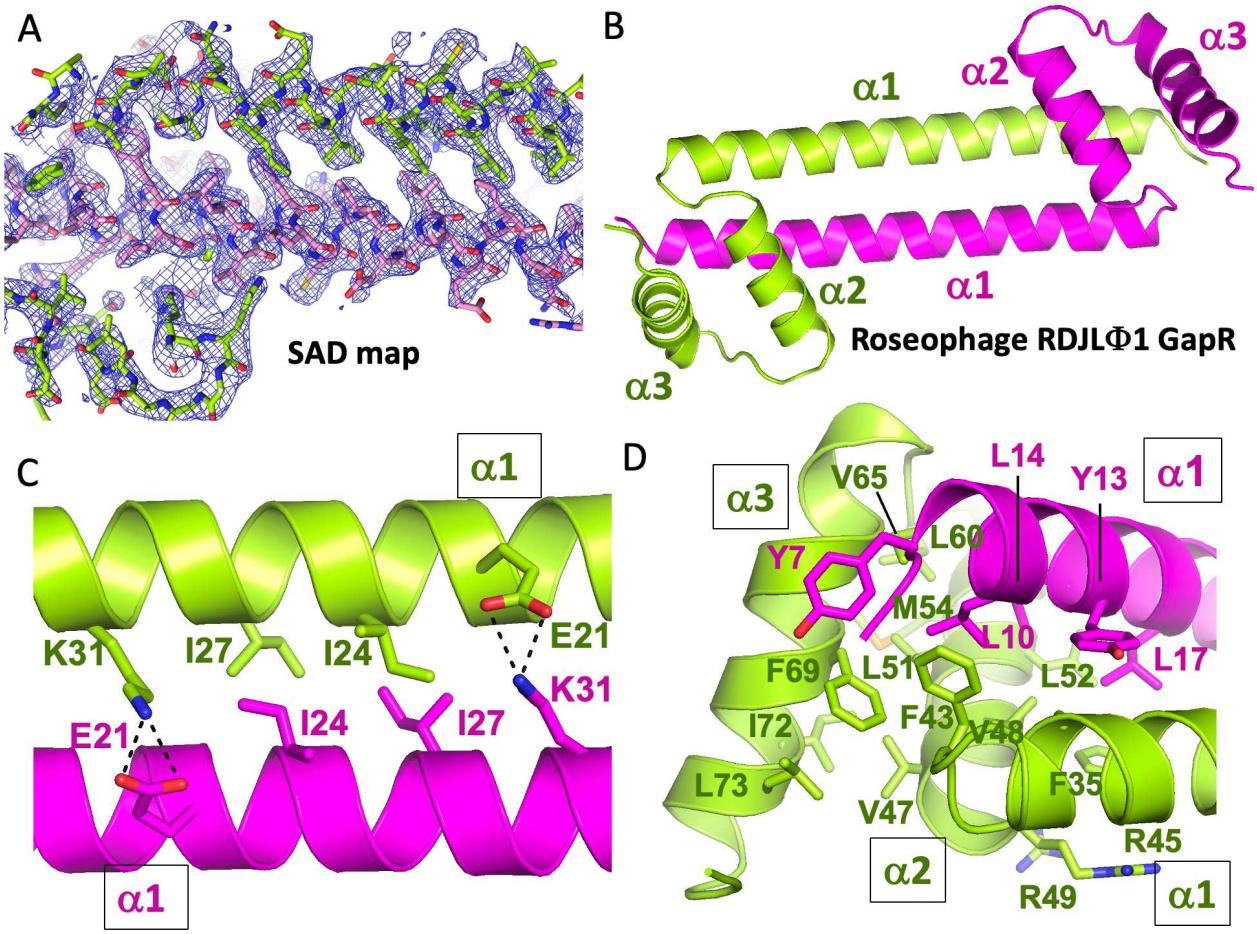
A
SAD map
B
α1
α2
α3
α2
α1
α3
Roseophage RDJLΦ1 GapR
C
α1
K31
I27
I24
E21
E21
I24
I27
K31
α1
D
α3
V65
L14
Y13
α1
Y7
L60
M54
L10
L17
F69
L51
L52
I72
F43
V48
L73
V47
F35
R45
α2
R49
α1

Figure 3

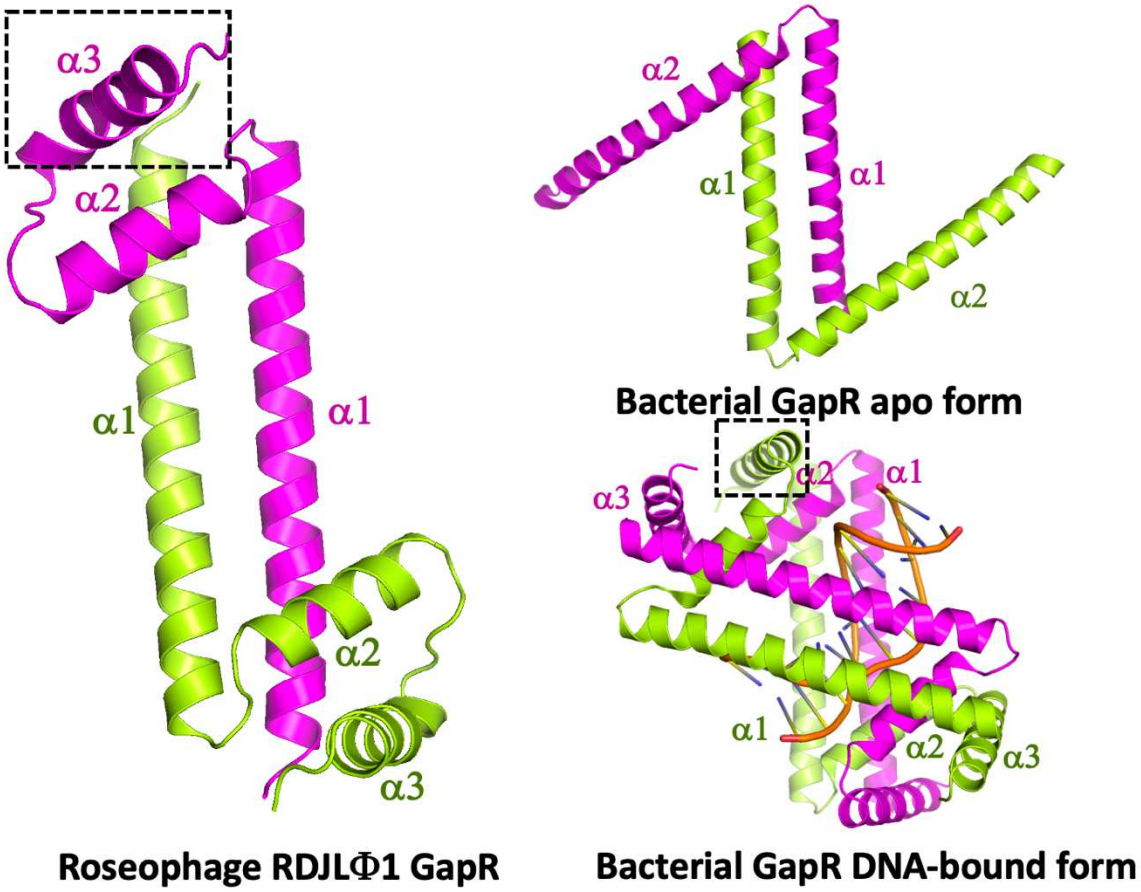
α3
α2
α1
α1
α2
α3
Roseophage RDJLΦ1 GapR
α2
α1
α1
α2
Bacterial GapR apo form
α3
α2
α1
α1
α2
α3
Bacterial GapR DNA-bound form

Figure 4

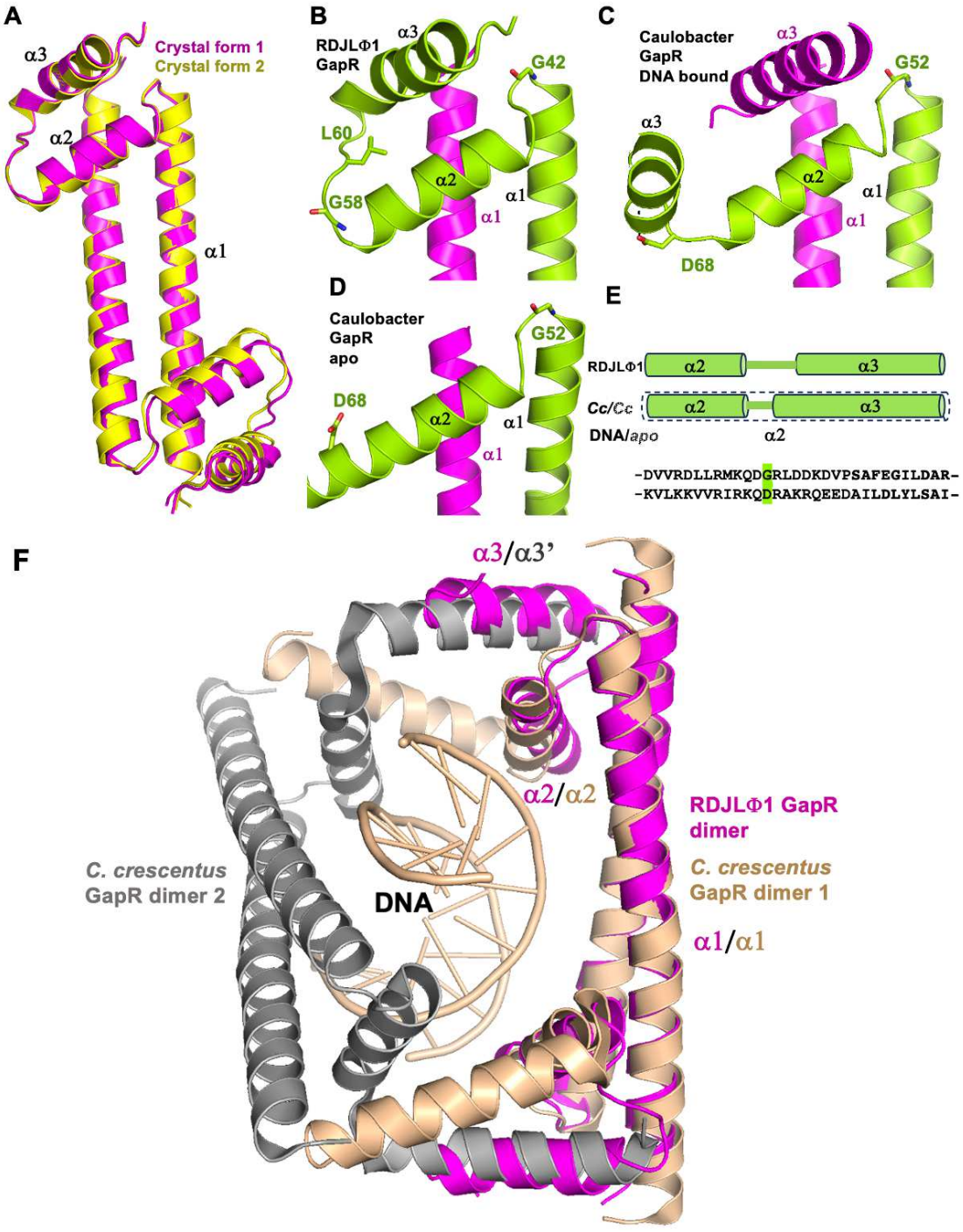
A
α3
α2
α1
Crystal form 1
Crystal form 2
B
RDJLΦ1
GapR
α3
G42
L60
G58
α2
α1
α1
C
Caulobacter
GapR
DNA bound
α3
G52
α3
α2
α1
α1
D68
D
Caulobacter
GapR
apo
G52
D68
α2
α1
α1
E
RDJLΦ1
α2
α3
Cc/Cc
α2
α3
DNA/apo
α2
-DVVRDLLRMKQDGRLDDKDVPSAFEGILDAR-
-KVLKKVVRIRKQDRAKRQEEDAILDLYLSAI-
F
α3/α3'
α2/α2
DNA
C. crescentus
GapR dimer 2
RDJLΦ1 GapR
dimer
C. crescentus
GapR dimer 1
α1/α1

Figure 5

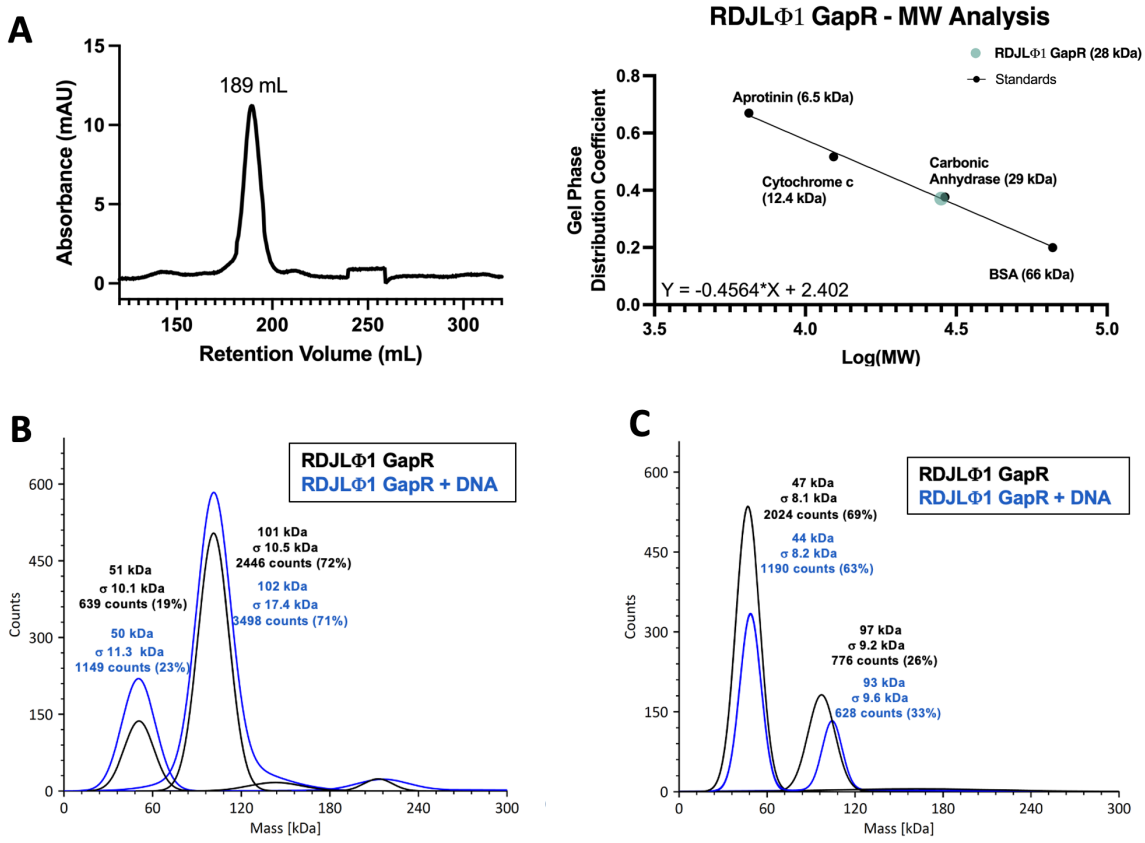
A
189 mL
Absorbance (mAU)
Retention Volume (mL)
RDJLΦ1 GapR - MW Analysis
RDJLΦ1 GapR (28 kDa)
Standards
Aprotinin (6.5 kDa)
Cytochrome c (12.4 kDa)
Carbonic Anhydrase (29 kDa)
BSA (66 kDa)
Y = -0.4564*X + 2.402
Gel Phase Distribution Coefficient
Log(MW)
B
RDJLΦ1 GapR
RDJLΦ1 GapR + DNA
51 kDa
σ 10.1 kDa
639 counts (19%)
50 kDa
σ 11.3 kDa
1149 counts (23%)
101 kDa
σ 10.5 kDa
2446 counts (72%)
102 kDa
σ 17.4 kDa
3498 counts (71%)
Counts
Mass [kDa]
C
RDJLΦ1 GapR
RDJLΦ1 GapR + DNA
47 kDa
σ 8.1 kDa
2024 counts (69%)
44 kDa
σ 8.2 kDa
1190 counts (63%)
97 kDa
σ 9.2 kDa
776 counts (26%)
93 kDa
σ 9.6 kDa
628 counts (33%)
Counts
Mass [kDa]

Figure 6

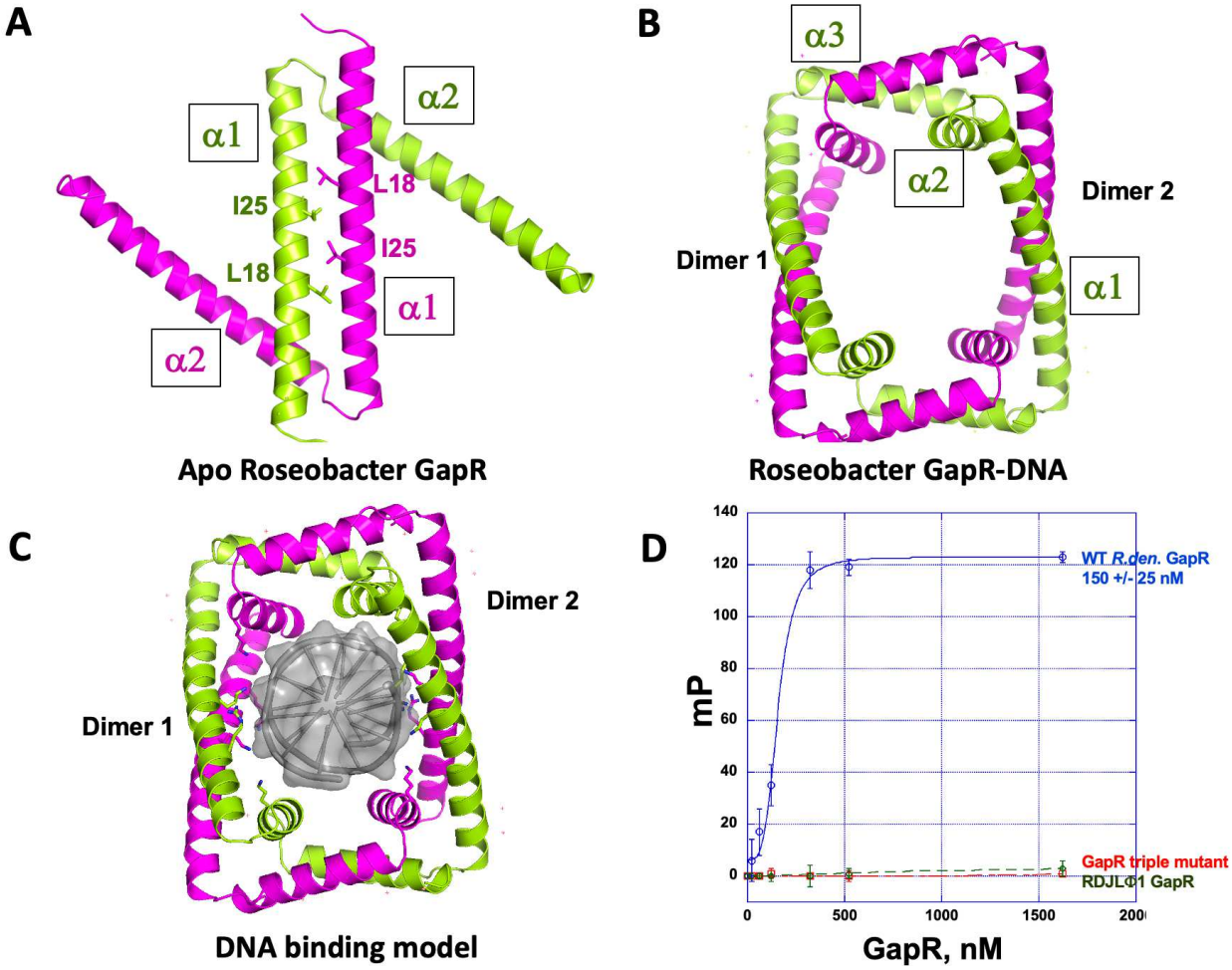
A
α1
α2
I25
L18
L18
I25
α1
α2
Apo Roseobacter GapR
B
α3
α2
Dimer 2
Dimer 1
α1
Roseobacter GapR-DNA
C
Dimer 2
Dimer 1
DNA binding model
D
140
120
100
80
60
40
20
0
mP
0
500
1000
1500
200
GapR, nM
WT R.den. GapR
150 +/- 25 nM
GapR triple mutant
RDJLΦ1 GapR

Figure 7

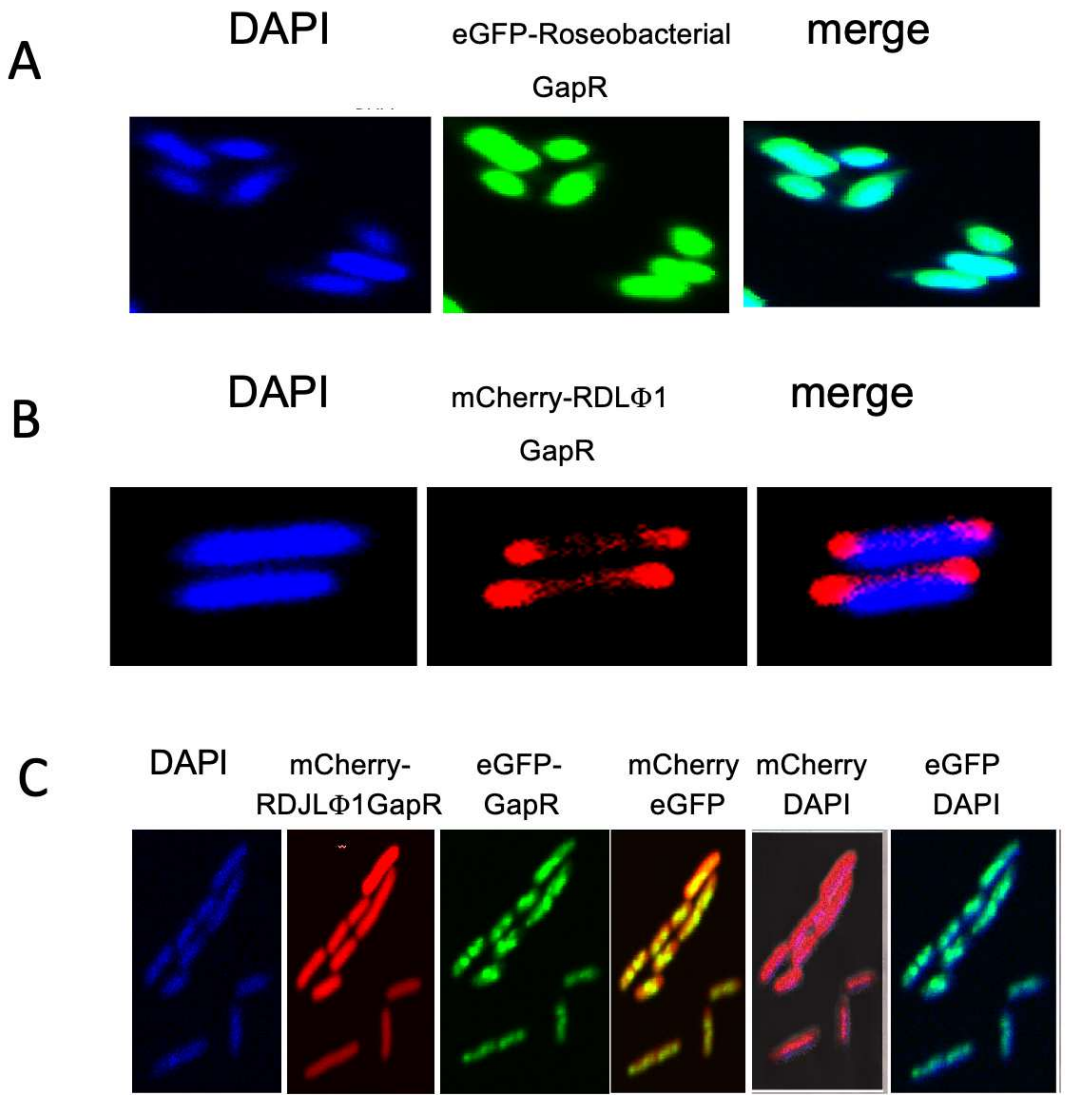
A
DAPI
eGFP-Roseobacterial GapR
merge
B
DAPI
mCherry-RDLΦ1 GapR
merge
C
DAPI
mCherry-RDJLΦ1GapR
eGFP-GapR
mCherry eGFP
mCherry DAPI
eGFP DAPI

Figure 8

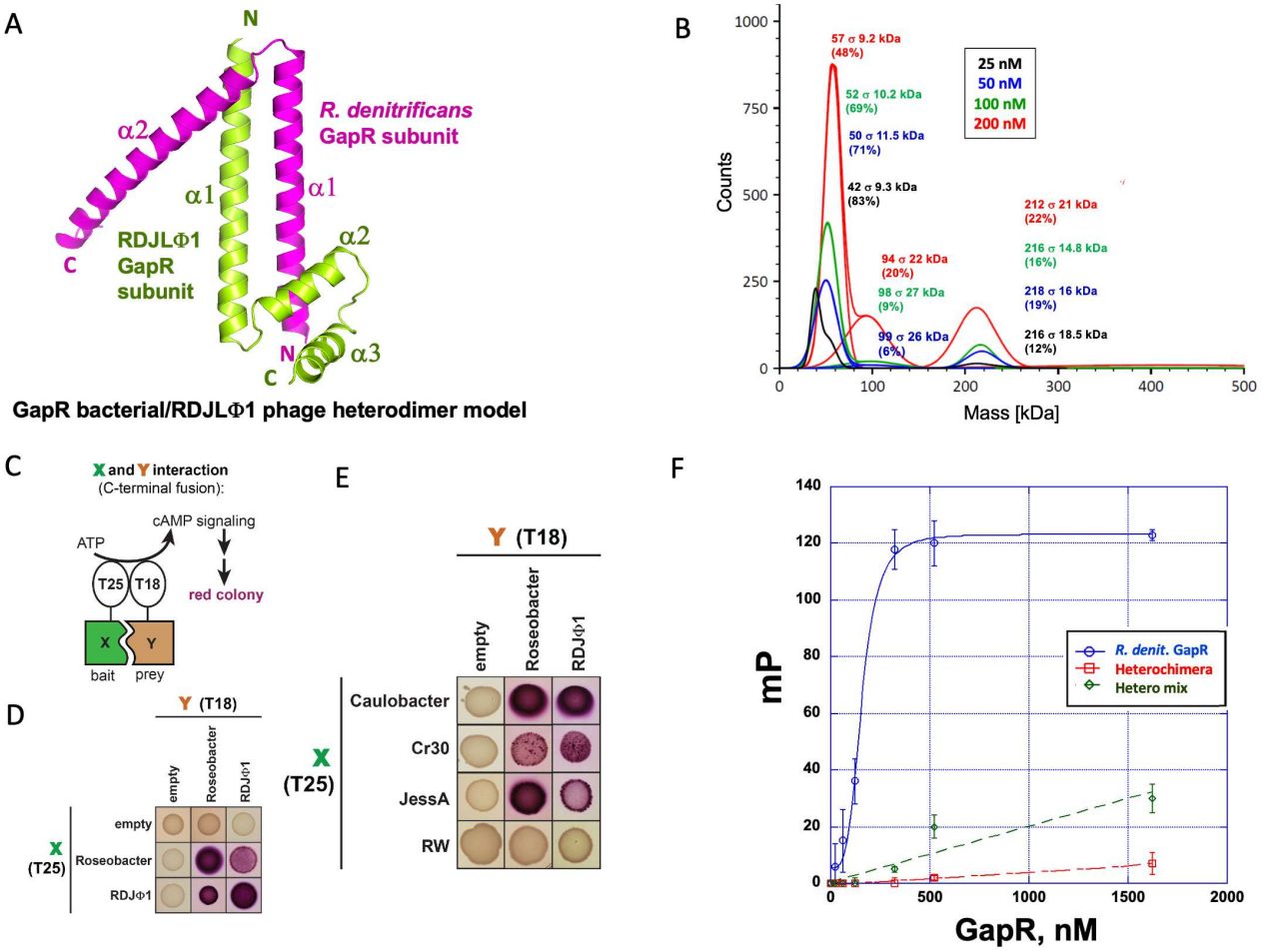
A
N
α2
α1
R. denitrificans
GapR subunit
α1
RDJLΦ1
GapR
subunit
α2
C
N
α3
C
GapR bacterial/RDJLΦ1 phage heterodimer model
B
Counts
Mass [kDa]
25 nM
50 nM
100 nM
200 nM
57 σ 9.2 kDa (48%)
52 σ 10.2 kDa (69%)
50 σ 11.5 kDa (71%)
42 σ 9.3 kDa (83%)
94 σ 22 kDa (20%)
98 σ 27 kDa (9%)
99 σ 26 kDa (6%)
212 σ 21 kDa (22%)
216 σ 14.8 kDa (16%)
218 σ 16 kDa (19%)
216 σ 18.5 kDa (12%)
C
X and Y interaction
(C-terminal fusion):
cAMP signaling
ATP
T25
T18
red colony
X
Y
bait
prey
D
Y (T18)
empty
Roseobacter
RDJΦ1
X (T25)
E
Y (T18)
Caulobacter
Cr30
JessA
RW
F
mP
GapR, nM
R. denit. GapR
Heterochimera
Hetero mix

Figure 9

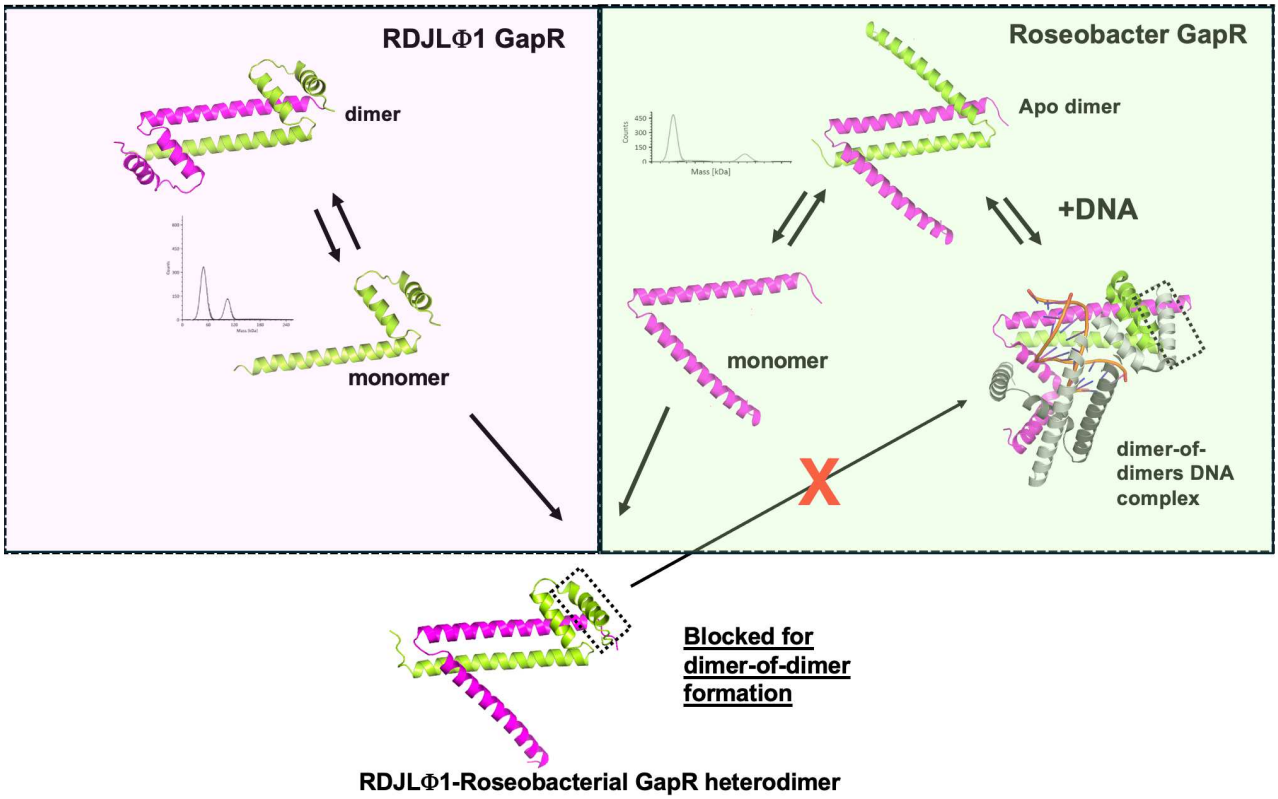
RDJLΦ1 GapR
dimer
monomer
Roseobacter GapR
Apo dimer
+DNA
monomer
dimer-of-dimers DNA complex
X
Blocked for dimer-of-dimer formation
RDJLΦ1-Roseobacterial GapR heterodimer

Supplementary Files

This is a list of supplementary files associated with this preprint. Click to download.

- NatcommSILASTFEB8Roseophage.pdf